Could Redox-Switched Binding of a Redox-Active Ligand to a Copper(II) Centre Drive a Conformational Proton Pump Gate? A Synthetic Model Study

Zhicong He, Stephen B. Colbran,* and Donald C. Craig[a]

Abstract: A proposal for a redox-linked conformational gate to proton translocation—a proton pump gate—based upon a transition-metal redox-switchable hemilabile ligand (RHL) system is made. Consideration of the requirements for such a system reveals copper(II) to be the ideal metal centre. To test the proposal and, thereby, to provide an artificial proton pump gate, the copper coordination chemistry of three tris(pyridylmethyl)amine (tpa) ligands with one "leg" (PY*) substituted at the 6-position of the pyridine ring by a dimethoxyphenyl (L^1), a hydroquinone (H_2L^2) or a quinone (L^3) substituent has been investigated. Crystal structures of *sp*-[Cu(κ^4N-L^1)Cl]Cl·3 H_2O (*sp* = square pyramidal), *sp*-[Cu(κ^3N-H_2L^2)-Cl_2] and *tbp*-[Cu(κ^4N,κO-HL^2)][PF_6] (*tbp* = trigonal bipyramidal) have been determined. The Cu^I complexes [Cu(L)$(MeCN)_n]^+$ (L = L^1, H_2L^2) display physicochemical properties consistent with a "dangling" PY* leg; from the NMR spectra, the barriers to inversion of the ligand amine donor for the Cu^I complexes are estimated to be within the range of about 30–45 kJ mol^{-1}. In the Cu^{II} complexes, coordination of the PY* leg is finely balanced and critically depends on the nature of the PY* substituent and the availability of potential co-ligand(s). For example, *tbp*-[Cu(κ^4N-L^1)Cl]$^+$ reacts cleanly with Cl^- ions to afford *sp*-[Cu(κ^3N-L^1)Cl_2]; Vis/NIR spectrophotometric titrations suggest the affinity of *tbp*-[Cu(κ^4N-L^1)Cl]$^+$ for Cl^- ion in dichloromethane is 9.7×10^2 and is at least 10^4-fold greater than that of *tbp*-[Cu(κ^4N-L^3)Cl]$^+$. The complex *sp*-[Cu(κ^3N-H_2L^2)Cl_2] has a "dangling" PY* leg, in which an intramolecular OH(hydroquinone)···N(pyridine) hydrogen bond "ties-up" the pyridyl nitrogen atom, and reacts with Brønsted bases to give *tbp*-[Cu(κ^4N,κO-HL^2)]$^+$. Two-electron oxidation of *sp*-[Cu(κ^3N-H_2L^2)Cl_2] is linked to loss of two protons and a conformational change, and affords *tbp*-[Cu(κ^4N-L^3)Cl]$^+$. The [Cu(κ^3N-H_2L^2)Cl_2] – [Cu(κ^4N-L^3)Cl]$^+$ system provides a first demonstration of the critical step in the proposed proton pumping cycle, namely a redox-driven and proton-linked conformational change. The possible biological relevance of this work to proton pumping in cytochrome *c* oxidase is mentioned.

Keywords: bioinorganic chemistry · copper · molecular devices · N ligands · proton transport

Introduction

Proton pumps are remarkable molecular machines capable of translocating protons across a membrane against a proton gradient,[1, 2] and are vitally important for all life since the transmembrane proton gradient created by the proton pumping proteins of the respiratory or photosynthetic pathways drives the synthesis of ATP, the energy currency of all cells.[3] For example, cytochrome *c* oxidase, one inspiration for this study, is respiratory complex IV and uses the free energy released as oxygen is reduced by electrons supplied from cytochrome *c* to pump protons against the proton gradient across the inner mitochondrial or a bacterial membrane according to Equation (1).[3, 4] This is the last step in aerobic respiration and accounts for the vast majority of oxygen consumed by living organisms.

$$8H^+_{in} + O_2 + 4e^- \rightarrow 4H^+_{out} + 2H_2O \quad (1)$$

The essential components of a proton pump include the proton-conducting (H^+) channels, which convey protons through the membrane, and the proton pumping "gate", the vital element that drives the unidirectional translocation of protons.[2, 3] In real systems, for example proton pumping membrane proteins such as cytochrome *c* oxidase, the H^+ channels consist of (transient) chains of protonatable amino acid side chains and bound water molecules along which the protons can passively hop.[2, 3, 5] The proton pumping gate is the site where the energy released by a chemical process is used to drive the proton pumping; that is the proton pump gate is the element that couples the chemical process to vectorial proton transport. In cytochrome *c* oxidase, for

[a] Dr. S. B. Colbran, Z. He, D. C. Craig
School of Chemical Sciences
University of New South Wales
Sydney, NSW 2052 (Australia)
Fax: (+61) 2-9385-6141
E-mail: s.colbran@unsw.edu.au

Supporting information for this article is available on the WWW under http://www.chemeurj.org or from the author.

0947-6539/03/0901-0116 $ 20.00+.50/0

example, the binuclear heme $a_3 \cdots Cu_B$ catalytic centre for reduction of oxygen is also believed to be the proton pumping gate.[6, 7] Although the structure of this centre is known to atomic resolution[5, 8] and there is much information about the states and intermediates in the catalytic cycle,[4, 9, 10] how reduction of oxygen is actually coupled to proton pumping remains a contentious issue that has occasioned much recent, robust intellectual debate.[5, 9, 10] Two facts about cytochrome *c* oxidase are mentioned here because they influenced this work: Firstly, one of the three histidine ligands—which one is unknown—to the Cu_B^I ion in the fully reduced state of cytochrome *c* oxidase is more weakly bound than the others and can be displaced by Cl^- ion;[11] secondly, one of the histidine ligands (His240 in the numbering scheme for the bovine enzyme) to Cu_B is covalently linked to a tyrosine (Tyr244) side chain[5, 8]—the resulting imidazole-phenol cofactor has recently been shown to be redox-active and is the donor of one of the four electrons required to cleave oxygen when it binds the heme $a_3 \cdots Cu_B$ active site.[12] Also essential to redox-linked proton pumps—those driven by a redox reaction such as cytochrome *c* oxidase—are one or more electron transfer pathways,[13, 14] networks of appropriately aligned and coupled covalent and hydrogen bonds and through-space jumps, for delivery of electrons to the catalytic centre where the redox reaction takes place.

Artificial proton pumps offer exciting prospects for new technologies for energy conversion and storage.[1, 2] Great recent progress has been made in the design, synthesis, and understanding of artificial ion and proton-conducting channels[15] and of artificial electron-transfer pathways.[14, 16, 17] In stark contrast, the synthesis and cycling of an artificial proton pump gate are yet to be demonstrated.[1, 2] Perhaps closest is the demonstration of proton transport across the lipid bilayer membranes of artificial vesicles driven by illumination of a membrane-spanning, artificial photosynthetic triad in the presence of a lipid-soluble naphthaquinone.[17, 18] These devices, however, are not proton pumps, but photo-driven Mitchell loops[3] that rely on diffusion of the lipid-soluble naphthahydroquinone to transport the protons across the vesicle membrane. Herein we outline a proposal for a simple artificial redox-linked proton pump gate and describe our first attempts to engineer a synthetic chemical system that demonstrates the concept; the possible biological relevance of our results is also mentioned.

Concept: transition-metal–RHL complexes as redox-linked proton pump gates

Figure 1 diagrammatically depicts a proposal for a proton pump that has a transition-metal centre bound by a redox-switchable hemilabile ligand (RHL)[19–22] as the proton pump gate. RHLs are ligands in which the binding to a metal centre of one of the donor groups is modulated by a covalently linked redox centre. The essential features of this proton pump gate are: 1) the discrete conformations for each redox-state of the RHL transition-metal centre; 2) the proton-dependent redox couple as the RHL redox-switch; 3) the fixed orientation for the RHL–transition-metal assembly, for example within a membrane protein, with respect to the membrane across which protons are to be pumped. Inductive withdrawal of electron density upon oxidation of the RHL redox centre weakens the binding of the covalently linked donor group ($L_{str} \rightarrow L_{wk}$), and it may be displaced from the metal centre by other ancillary ligand(s), provided these are available (conformation **I** → conformation **II** in Figure 1). Reduction of the ligand redox centre increases the nucleophilicity of the donor group ($L_{wk} \rightarrow L_{str}$) that rebinds to the metal centre (conformation **II** → conformation **I** in Figure 1). The concept of

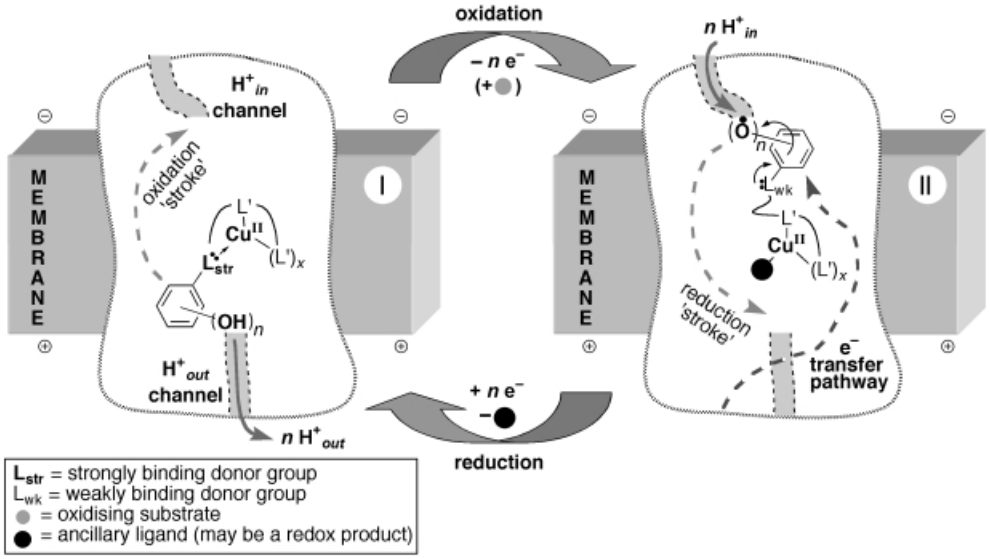

Figure 1. Cartoon of the proposed conformational proton pump cycle highlighting the role of the Cu^{II}–RHL centre as the redox-linked proton pumping gate. Starting with the metal centre in conformation **I** (left-side), RHL-centred oxidation releases protons through the exit H^+ channel and creates a weaker donor group (L_{wk}) that is displaced by ancillary ligand(s) and swings away (the dashed arrow marked "oxidation stroke") so that the Cu^{II}–RHL centre adopts conformation **II** (right-side). RHL-centred reduction in conformation **II** is tightly linked to uptake of protons through the input H^+ channel and creates a stronger donor group (L_{str}) that moves to rebind the Cu^{II} ion (the dashed arrow marked "reduction stroke") thus regenerating **I**. Protons are only carried by the RHL during the "reduction stroke", thereby leading to vectorial transport of protons from the input to the exit H^+ channels. For further details, see the text.

  0947-6539/03/0901-0117 $ 20.00+.50/0

RHLs was first demonstrated by ourselves for phosphinoquinone/hydroquinone RHLs[19, 20] and by Mirkin and co-workers for ferrocene/ferrocenium-substituted RHLs.[21] As the RHL redox-switch in the proposed proton pumping gate is a proton-dependent couple, oxidation and reduction are accompanied by proton release and uptake in two discrete conformational states, one for output and one for input of electrons and protons. The protons enter and leave the active centre through two (or more) H^+ channels. Redox-linked movement of the hemilabile donor group connects the input and output H^+ channels and, since only the reduced state of the redox-switch carries protons, allows only unidirectional movement of protons. As depicted the movement of the labile ligand group is exaggerated, for in a real system proton tunnelling at comparable energies to electron transfer is unlikely over distances greater than 0.25 Å.[23] The labile ligand group, therefore, need only move about 0.3 Å to gate proton movement, with any remaining distance between input and exit channels spanned by a (transitory) hydrogen-bonded chain of protonatable groups (e.g. protein residues or water molecules) along which protons passively hop. Electrons are supplied to/from the redox centre by a separate electron transfer pathway(s), and electron transfer may be coupled to the movement of one or more protons along an H^+ channel (represented in Figure 1 by the crossover of the proton and electron pathways). Cycling between conformers **I** and **II** leads to vectorial translocation of protons linked to the redox changes at the RHL–transition-metal centre. An oxidising substrate could oxidise the redox centre of the ligand, in which case the electron-transfer pathway need only deliver electrons, and the reduction product(s) of the substrate may be the ancillary ligand(s) that displaces the oxidised form (L_{wk}) of the ligand-donor group in conformer **II**. The principle remains the same for any proton-dependent redox couple as the RHL redox switch.

System requirements and choice of synthetic models

For proof of this concept, we sought to demonstrate for a synthetic model system, a transition-metal complex of a proton-dependent RHL, that the ligand redox switch could control the binding of the hemilabile donor to the metal ion, with oxidation and reduction of the ligand redox centre accompanied by proton loss and uptake at different spatial locations with respect to the metal centre. There are several requirements for the transition metal and the proton-dependent RHL that led to a target system.

1) *The metal ion* should exhibit fast exchange reactions so that the hemilabile donor group can rapidly cycle on/off. The other RHL donor group(s) should remain strongly bound to the metal. These conditions lead naturally to Cu^{II} ion. Although Cu^{II} ion exhibits the largest formation constants for the first d series divalent ions (the Irving–Williams series),[24] it also exhibits the fastest rates for transition metal ions because Jahn–Teller effects lead to weak binding of ligand(s) along (at least) one axis.[25]
2) *The RHL* must be flexible and coordination of the ligand group substituted by the redox-centre to the metal ion should be finely balanced. In a proton pumping enzyme this would be dictated by the protein structure. For models, we targeted copper complexes of new tris(pyridylmethyl)-amine (tpa) ligands derivatised with proton-dependent redox centres. There were two reasons for this choice. Firstly, tpa and derivatives are flexible and usually form copper complexes exhibiting κ^4N-coordination, but κ^3N-coordination with one pyridyl leg unbound, "dangling" away from the copper centre is also found, especially with more sterically encumbered pyridyl groups.[26] Secondly, with a view to later studies of the reactions of Cu^I complexes with dioxygen, we noted that copper–tpa complexes are commonly used to model the copper centres in dioxygen binding/utilising copper proteins,[27] including cytochrome *c* oxidases,[28] and promote formation of end-on rather than side-on dioxygen adducts (the Cu_B ion in the resting, oxidised state of cytochrome *c* oxidase may be bound by end-on peroxide[5]).
3) *The RHL redox switch* must exhibit a proton-dependent redox couple that must perturb the binding of a ligand donor group to the metal centre. Both partners of the ($2e^-$, $2H^+$) *p*-quinone–*p*-hydroquinone redox couple are stable[19, 20, 29, 30] and, therefore, the (hydro)quinone group is an ideal first choice for the RHL redox centre. Direct attachment of the redox centre to a pyridyl ring of tpa serves the dual functions of modulation of the binding ability of the pyridyl ring and providing the steric bulk to direct binding of this pyridyl ring to along the weak field axis in a Cu^{II} complex. Chloride ion was chosen as the coligand/counterion, in part, because of the evidence for Cl^- ion displacing a histidine ligand to the Cu_B centre in cytochrome *c* oxidases.[11]

In sum these requirements led us to investigate the copper coordination chemistry of H_2L^2, L^3 and, for comparison, L^1, as reported herein.

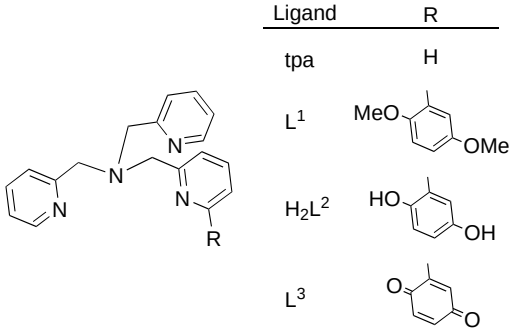

Results

Syntheses: The ligands L^1 and H_2L^2 were prepared as follows. 1,4-Dimethoxybenzene or 1,4-di(tetrahydropyranyloxy)benzene were treated with 1.1 equivalents of *n*-butyllithium to generate the monolithio species that were allowed to react with tri(isopropyl)boron to give borate intermediates, which were treated directly in the same pot with 6-bromopyridine-2-carboxaldehyde under Suzuki coupling conditions to afford the corresponding 6-aryl-pyridine-2-carboxaldehydes in

0947-6539/03/0901-0118 $ 20.00+.50/0 *Chem. Eur. J.* **2003**, *9*, No. 1

about 70% yield. These were coupled with di(2-pyridylmethyl)amine using sodium triacetoxyborohydride.[31] L^1 was obtained in 70% yield and, following treatment with ethanol–HCl (pH 3) to remove the tetrahydropyranyl protecting groups, H_2L^2 was obtained in about 60% yield.

The Cu^{II} complexes, deep blue $[Cu(L^1)Cl]Cl$ (**1**) and jade-green $[Cu(H_2L^2)Cl_2]$ (**3**), crystallised directly from solutions of the appropriate ligand and $CuCl_2 \cdot 2H_2O$ in dry methanol (for **1**) or dry ethanol (for **3**) that were placed under atmospheres of dry diethyl ether. All procedures and measurements involving **3** were performed under strictly anaerobic conditions, because solutions of **3** decomposed upon exposure to oxygen or moisture, but were indefinitely stable in dry, deoxygenated solvents; attempts to identify the brown oxidation product(s) obtained upon bubbling dry oxygen through solutions of **3** were unsuccessful.[32] Treatment of **1** with excess $K[PF_6]$ in methanol gave deep indigo-blue $[Cu(L^1)Cl][PF_6]$ (**2**) in near quantitative yield. The blue *p*-quinonyl-substituted complex, $[Cu(L^3)Cl]Cl$ (**4**), was obtained by oxidation of **3**. Three methods were employed: a) treatment of **3** in acetonitrile solution with two equivalents of $[NH_4]_2[Ce(NO_3)_6]$; b) treatment of **3** in dichloromethane or acetone solutions with one equivalent of 2,3-dicyano-5,6-dichlorobenzoquinone (DDQ); c) exhaustive controlled potential electrolysis of **3** in acetonitrile – 0.2 M $[NBu_4][PF_6]$ with the potential poised at +0.47 V, just above that of the anodic peak for the oxidation of the hydroquinone group in the cyclic voltammogram of **3** (see below). The characteristic green colour of solutions of **3** turned to blue as the oxidations to **4** proceeded. The samples of **4** obtained by the three methods displayed identical spectroscopic properties (see below). Reaction of **3** in dry methanol with one equivalent of NaOH, followed by metathesis with $K[PF_6]$ gave a dark brown solution, which afforded lustrous golden-brown crystals of $[Cu(HL^2)][PF_6]$ (**5**) when left to stand under a diethyl ether atmosphere.

The Cu^{I} complexes, $[Cu(L^1)(MeCN)_x][PF_6]$ (**6**) and $[Cu(H_2L^2)(MeCN)_x][PF_6]$ (**7**), were prepared by three methods: a) mixing equivalent amounts of the appropriate ligand (L^1 or H_2L^2) and $[Cu(MeCN)_4][PF_6]$ together in acetonitrile solution; b) reduction of the corresponding Cu^{II} complex, **1** or **3**, with one equivalent of cobaltocene in acetonitrile; c) exhaustive controlled potential reductions of **1** in acetonitrile – 0.2 M $[NBu_4][PF_6]$, which consumed about 1.0 Faraday mol^{-1}. A controlled potential electrolysis of **3** at −0.9 V resulted in decomposition and deposition of copper metal. Likewise, attempts to concentrate solutions containing **7** caused disproportionation/decomposition and a pure solid sample of this complex was not obtained. Solutions of **6** and, particularly, **7** were not stable, decomposing rapidly in chlorinated solvents and more slowly in acetonitrile (within several hours), and were extremely dioxygen sensitive. Details of the reactions of **6** and **7**, which are not the subject of the present investigation, will be reported elsewhere.[33] It is noteworthy, however, that the reaction of **7** in dry acetone with dioxygen at −90 °C produced a dark-brown intermediate species that cleanly decomposed upon warming to give **5** in about 75% yield with hydrogen peroxide detected as a coproduct.

Crystal structures: The X-ray crystal structure of $[Cu(\kappa^4N\text{-}L^1)Cl]Cl \cdot 3H_2O$ (**1** $\cdot 3H_2O$; Figure 2) reveals two independent but near identical Cu^{II} complex ions (A and B), each bound by the three pyridyl and the amine donor groups of L^1 and by a

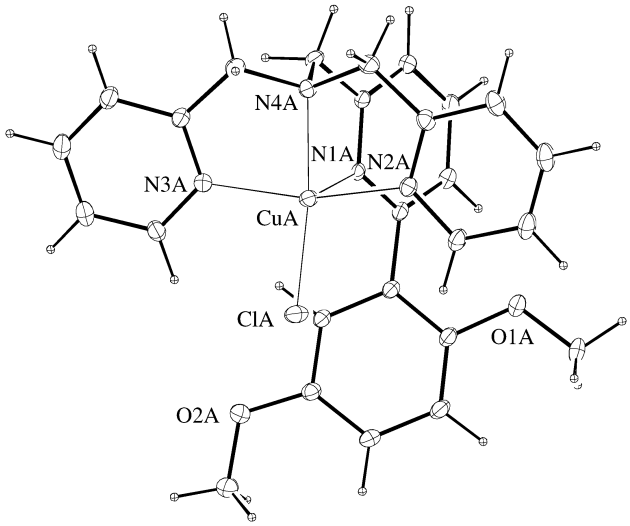

Figure 2. View of cation A from the crystal structure of $[Cu(L^1)Cl]Cl \cdot 3H_2O$ (**1**) (10% thermal ellipsoids shown). Key bond lengths [Å] and angles [°]: CuA–ClA 2.232(3), CuA–N1A 2.351(6), CuA–N2A 1.991(6), CuA–N3A 1.996(6), CuA–N4A 2.052(8); ClA-CuA-N1A 117.3(2), ClA-CuA-N2A 96.7(2), ClA-CuA-N3A 94.5(2), ClA-CuA-N4A 162.6(3), N1A-CuA-N2A 85.9(2), N1A-CuA-N3A 103.0(2), N1A-CuA-N4A 80.1(3), N2A-CuA-N3A 160.5(3), N2A-CuA-N4A 83.1(3), N3A-CuA-N4A 81.4(3). Data for cation B: CuB-ClB 2.234(3), CuB-N1B 2.362(6), CuB-N2B 1.994(5), CuB-N3B 2.000(5), CuB-N4B 2.045(7); ClB-CuB-N1B 119.8(2), ClB-CuB-N2B 95.9(2), ClB-CuB-N3B 94.1(2), ClB-CuB-N4B 160.5(3), N1B-CuB-N2B 88.3(2), N1B-CuB-N3B 101.4(2), N1B-CuB-N4B 79.7(3), N2B-CuB-N3B 160.3(3), N2B-CuB-N4B 82.9(3), N3B-CuB-N4B 82.1(3).

chloro coligand. The Cu^{II} ions adopt square-pyramidal (*sp*) geometries (cation A: τ[34] = 0.03; cation B: $\tau < 0.01$) with the bulky aryl-substituted pyridyl (PY*) group directed to the axial position at an average Cu–N distance of 2.353 Å, substantially longer than the equatorial Cu–N distances (av 2.030 Å). The Cu–Cl distances are normal and average 2.294 Å. In the crystal structure, the Cl^- counterions and the three water molecules are disordered over four sites, well isolated from the cations. The only notable inter-cation interaction in the crystal structure is offset π-stacking at about 3.5 Å between the dimethoxyphenyl rings of the bulky PY* legs of the pairs of molecules A and B. The crystal structure of $[Cu(\kappa^4N\text{-}L^1)Cl][PF_6]$ (**2**), which exhibits *sp*-$[Cu(\kappa^4N\text{-}L^1)Cl]^+$ ions ($\tau = 0.15$) similar to those found for **1**, is reported elsewhere along with those of L^1 and seven other first d-series metal complexes of this ligand.[33]

Immediately apparent from the X-ray crystal structure of **3** (Figure 3) is that the complex is $[Cu(\kappa^3N\text{-}H_2L^2)Cl_2]$ with the PY* leg uncoordinated and orientated away from the Cu^{II} ion, its place taken by a second chloro coligand such that the complex is *sp* ($\tau = 0.03$). An intramolecular hydrogen bond between the hydroquinonyl 2-OH group and the pyridine N atom (O1 ··· N1 2.559 Å) "ties up" the PY* leg. The three equatorial Cu–N (av 2.022 Å) and the equatorial Cu–Cl

  0947-6539/03/0901-0119 $ 20.00+.50/0

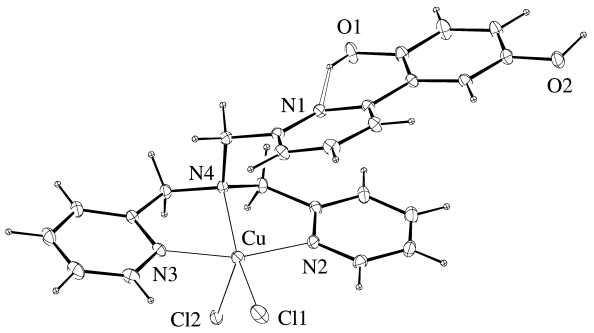

Figure 3. View of crystal structure of $[Cu(H_2L^2)Cl_2]$ (**3**) (10% thermal ellipsoids shown). Key bond lengths [Å] and angles [°]: Cu–Cl1 2.225(1), Cu–Cl2 2.585(1), Cu–N2 2.011(3), Cu–N3 2.004(3), Cu–N4 2.052(3); Cl1-Cu-Cl2 106.3(1), Cl1-Cu-N2 97.5(1), Cl1-Cu-N3 97.8(1), Cl1-Cu-N4 160.4(1), Cl2-Cu-N2 92.9(1), Cl2-Cu-N3 91.5(1), Cl2-Cu-N4 93.3(1), N2-Cu-N3 162.3(1).

(2.225(1) Å) bond lengths are normal and comparable to those found in **1**; in contrast, the axial Cu–Cl bond is longer (2.582(1) Å). The overall structure of **3** is similar to that of $[Zn(\kappa^3N\text{-}L^1)Cl_2]$,[33] but there are significant differences in the detail: for example, the Zn^{II} complex exhibits appreciably longer metal–N bond lengths (Zn–N av 2.210 Å), near equal Zn–Cl bond lengths (2.235(1) and 2.244(1) Å), and considerable trigonal distortion about the Zn^{II} centre ($\tau = 0.29$).

The crystal structure of **5** (Figure 4) reveals that the 2,5-hydroquinonyl-substituent of H_2L^2 binds to the Cu^{II} ion as a 2-hydroquinonate O-donor along with the four nitrogen atoms of the ligand. The $[Cu(\kappa^4N,\kappa O\text{-}HL^2)]^+$ ion adopts a distorted trigonal-bipyramidal (*tbp*) geometry ($\tau = 0.71$) with the amine N atom and the hydroquinonate O atom in the axial positions and the three pyridyl groups equatorial. Constrained by the ligand design, the distances from the Cu center to the donor atoms of the PY* arm (Cu1–O2 1.899(4) Å and Cu1–N4 1.978(4) Å) are significantly shorter than the other coordinate bonds. The structure of **5** resembles that of $[CuL^4][ClO_4]$ (L^4 = bis(2-aminoethyl)(2-(4′-nitro-2′-hydroxyphenyl)iminoethyl)amine),[35] and analogous $\kappa^4N,\kappa O$-binding of a phenolate-tpa ligand was recently found in $[Fe_2(6\text{-}(2\text{-phenolato})\text{-tpa})_2(\mu\text{-O})]^{2+}$, although to an octahedral Fe^{III} ion in this case.[36]

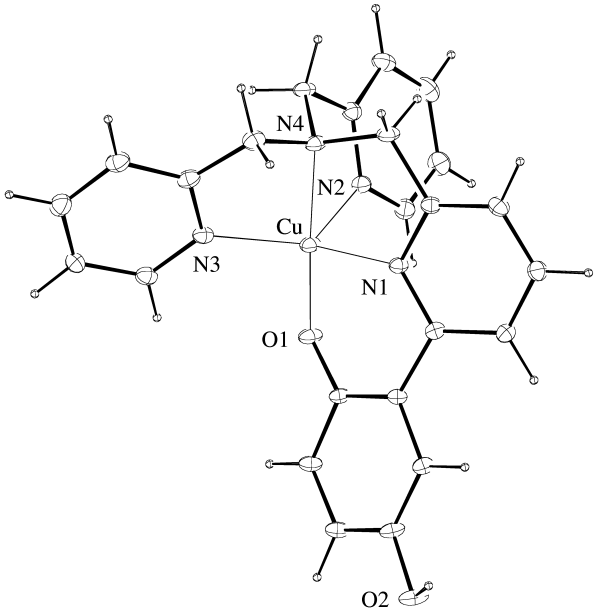

Figure 4. View of the cation from the crystal structure of $[Cu(HL^2)][PF_6]$ (**5**) (10% thermal ellipsoids shown). Key bond lengths [Å] and angles [°]: Cu–O1 1.899(4), Cu–N1 1.978(4), Cu–N2 2.129(5), Cu–N3 2.019(5), Cu–N4 2.041(4); O1-Cu-N1 94.9(2), O1-Cu-N2 96.1(2), O1-Cu-N3 100.7(2), O1-Cu-N4 175.8(2), N1-Cu-N2 98.1(2), N1-Cu-N3 133.2(2), N1-Cu-N4 84.8(2), N2-Cu-N3 123.4(2), N2-Cu-N4 79.8(2), N3-Cu-N4 82.5(2).

Physicochemical properties

Copper(II) complexes: Emphasis is placed in the following description on establishing the structures of the complexes in solution and, where not known from X-ray crystallography, in the solid-state. All complexes gave correct partial elemental analyses.

Infrared spectra: Data for selected key bands from FTIR spectra recorded for the ground (micro)crystalline complexes in KBr disks are given in Table 1. Free pyridines show two ring deformation bands at about 1590–1580 and about 1575–1565 cm^{-1} with the higher energy band shifting to about 1615–1605 cm^{-1} upon coordination to a metal ion.[37] These bands are easily distinguished in the FTIR spectra of the complexes allowing the unambiguous assignment of the coordination mode of the tpa ligand, Table 1 and, for example, Figure 6. Also of note, FTIR spectra of **4** in solution and in the solid show a strong quinonyl carbonyl peak at 1662 cm^{-1}.

Table 1. Pyridine-ring deformation band data from the FTIR spectra of the solid complexes, and the deduced number of pyridine groups bound to the metal ion.

	$\tilde{\nu}_{PY+PY^*}$ [cm^{-1}]	N° of bound PY
$[Cu(L^1)Cl]Cl$ (**1**)	1608, 1573	3
$[Cu(L^1)Cl][PF_6]$ (**2**)	1609, 1581	3
$[Cu(H_2L^2)Cl_2]$ (**3**)	1608, 1596, 1567	2
$[Cu(L^3)Cl]Cl$ (**4**)	1613, 1564	3
$[Cu(HL^2)][PF_6]$ (**5**)	1608, 1567	3
$[Cu(L^1)][PF_6]$ (**6**)	1608, 1597, 1577	2
$[Zn(L^1)Cl_2]$[a]	1605, 1585, 1572	2

[a] Data from reference [33].

Conductivity: Table 2 presents molar electrical conductivity data obtained for 1.0 mM solutions of the complexes in anhydrous dichloromethane and in dimethylformamide. In

Table 2. Molar electrical conductivity values (±10%) for the complexes.

	Λ_M [$S\,cm^2\,mol^{-1}$]		
	CH_2Cl_2	dmf	CH_3OH
$[Cu(L^1)Cl]Cl$ (**1**)	4	44	[a]
$[Cu(L^1)Cl][PF_6]$ (**2**)	24	64	[a]
$[Cu(H_2L^2)Cl_2]$ (**3**)	6	42	192
$[Cu(L^3)Cl]Cl$ (**4**)	17	47	[a]
$[Cu(HL^2)][PF_6]$ (**5**)	22	59	80
$[Zn(L^1)Cl_2]$	4[b]	9[b]	[a]
$[NBu_4][PF_6]$	26	73	96

[a] Not measured. [b] Data from [33].

0947-6539/03/0901-0120 $ 20.00+.50/0 *Chem. Eur. J.* **2003**, *9*, No. 1

dichloromethane, the values are consistent with **1** and **3** behaving as non-electrolytes, and **2, 4** and **5** as 1:1 electrolytes. This suggests that in dichloromethane **1** is $[Cu(L^1)Cl_2]$, not $[Cu(L^1)Cl]^+Cl^-$ as found in the crystal structure, and **4** is $[Cu(L^3)Cl]^+Cl^-$ rather than $[Cu(L^3)Cl_2]$. In dimethylformamide, the molar conductivities are consistent with all copper complexes behaving as 1:1 electrolytes. Thus, in dimethylformamide the dichloride complexes are all $[Cu(L)Cl]^+Cl^-$ (**1**: $L = L^1$; **3**: $L = H_2L^2$; **4**: $L = L^4$). The lower conductivity values, in both solvents, when Cl^- is the counterion point to (stronger) ion pairing.

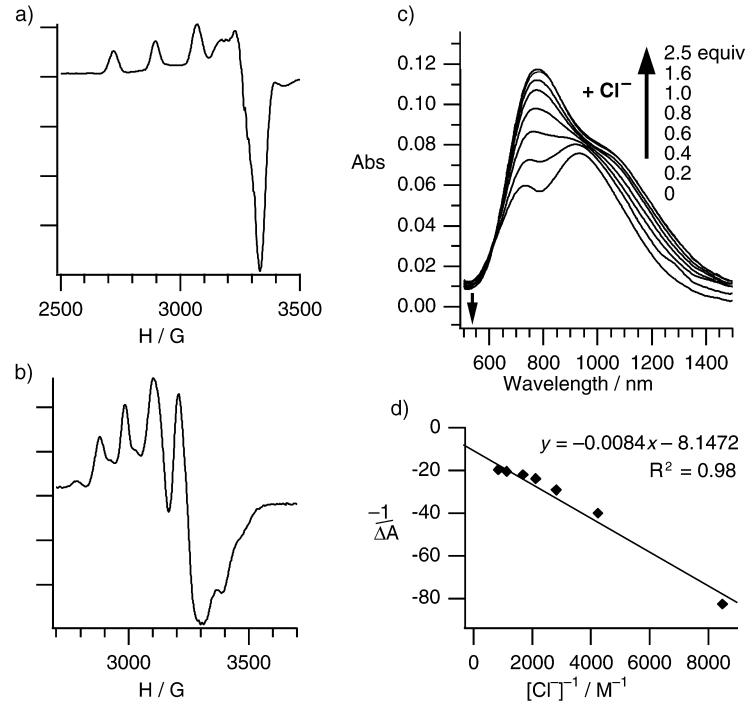

Figure 5. X-band EPR spectra of $[Cu(L^1)Cl_2]$ (**1**) (a) and $[Cu(L^1)Cl][PF_6]$ (**2**) (b) in frozen dichloromethane solution at 80 K. c, d). Titration of $[Cu(L^1)Cl][PF_6]$ (**2**, 0.59 M) with Cl^- ion in dichloromethane at 295 K to afford $[Cu(L^1)Cl_2]$ (**1**): Vis-NIR spectra (c) and the corresponding double-reciprocal plot ($-1/\Delta A$ versus $1/[Cl^-]_{added}$; ΔA = absorbance change at 735 nm) (d).

X-band EPR and UV/Vis/NIR spectra: Salient solution-state data are presented in Table 3. EPR spectra of **1** and **3** in dichloromethane or acetonitrile at 80 K show typical axial features with $g_\parallel > g_\perp > 2.0$ and $|A_\perp| \sim 170-180$ G indicative for tetragonally distorted ($d_{x^2-y^2}$ ground-state) elongated octahedral or *sp* Cu^{II} species in solution,[27, 38] whereas EPR spectra of **2, 4** and **5** in dichloromethane or acetonitrile have a typical "inverted axial" appearance with $g_\perp > g_\parallel \sim 2.0$ and $|A_\perp| \sim 115$—110 G $> |A_\parallel| \sim 85$ G indicative for (d_{z^2} ground-state) *tbp* species in solution,[27, 38] for example see Figures 5, 6, and the Supporting Information. The solid samples of **4** (and **5**) display "inverted axial" powder EPR spectra ($g_\perp \sim 2.014 > g_\parallel \sim 2.0$) at 80 K, which reveal **4** (and **5**) retains a *tbp* coordination geometry in the solid-state. In contrast, powdered samples of microcrystalline **1**–**3** exhibit rhombic EPR spectra ($g_1 \sim 2.2$, $g_2 \sim 2.1$, $g_3 \sim 2.0$) at 80 K. UV/Vis/NIR spectra of **1**–**4** in dichloromethane or acetonitrile solutions show intense ligand-centred bands below 350 nm, and weak d–d transitions in the Vis/NIR region with profiles[27, 38] characteristic for *sp* Cu^{II} centres for **1** and **3** and *tbp* Cu^{II} centres for **2** and **4** (Figure 5 and Figure 6). Spectra of **5** show intense ligand-centred bands below 350 nm, and a characteristic intense, sharp band at about 400 nm, which was not observed for the other complexes, along with three weak, broad shoulders to this at about 520, 660 and 930 nm (see Supporting Information).

Table 3. Electronic and X-band EPR spectroscopic data for the Cu^{II} complexes.

	UV-Vis-NIR (295 K)[a] λ_{max} [nm] (ε [$M^{-1}cm^{-1}$])	EPR (80 K)[a]
$[Cu(L^1)Cl_2]$ (**1**)	257 (17700), 320 (8000), 770 (200), 1050 (130)	$g_\parallel = 2.236$, $g_\perp = 2.027$, $A_\parallel = 176$ G
$[Cu(L^1)Cl][PF_6]$ (**2**)	259 (13800), 311 (5050), 730 (105), 930 (130)	$g_\perp = 2.235$, $g_\parallel \sim 2.0$, $A_\perp = 112$ G, $A_\parallel \sim 86$ G
$[Cu(H_2L^2)Cl_2]$ (**3**)[b]	253 (16400), 336 (3600), 720 (130), 855 (120)	$g_\parallel = 2.239$, $g_\perp = 2.025$, $A_\parallel = 171$ G
$[Cu(L^3)Cl]Cl$ (**4**)	246 (10500), 265 (9800), 730 (100), 900 (130)	$g_\perp = 2.228$, $g_\parallel \sim 2.0$, $A_\perp = 113$ G, $A_\parallel \sim 85$ G
$[Cu(HL^2)][PF_6]$ (**5**)	256 (13400), 286 (12000), 410 (4600), 520 (550), 650 (270), 1000 (90)	$g_\perp = 2.200$, $g_\parallel \sim 2.0$, $A_\perp = 115$ G, $A_\parallel = 84$ G

[a] In dichloromethane solution (unless stated otherwise). [b] $[Cu(H_2L^2)Cl_2]$ is poorly soluble in dichloromethane and the data for this complex are from spectra of anhydrous acetonitrile solutions.

Titrations with Cl^- ion: Figure 5c shows Vis/NIR spectra from a typical titration of **2** ($\lambda_{max} = 930$ nm) in dichloromethane with $[(Ph_3P)_2N]Cl$. An isosbestic point at 630 nm reveals a direct conversion from *tbp* reactant to *sp* product, **1** ($\lambda_{max} = 767$ nm), without intermediate species (Scheme 1). A plot of the absorbance change at 770 nm (ΔA_{770}) against the ratio of Cl^-:**2** indicates a single Cl^- ion binds to **2** (two Cl^- bind Cu overall), and the chloride affinity constant [K_{Cl}: Eq. (2)] at 295 K is estimated from the

$$[Cu(L)Cl]^+ + Cl^- \overset{K_{Cl}}{\rightleftharpoons} [Cu(L)Cl_2] \; (L = tpa, L^1, L^4) \qquad (2)$$

double reciprocal plot of the inverse of the absorbance change at 735 nm (ΔA_{735}) against the inverse of the Cl^- ion concen-

  0947-6539/03/0901-0121 $ 20.00+.50/0

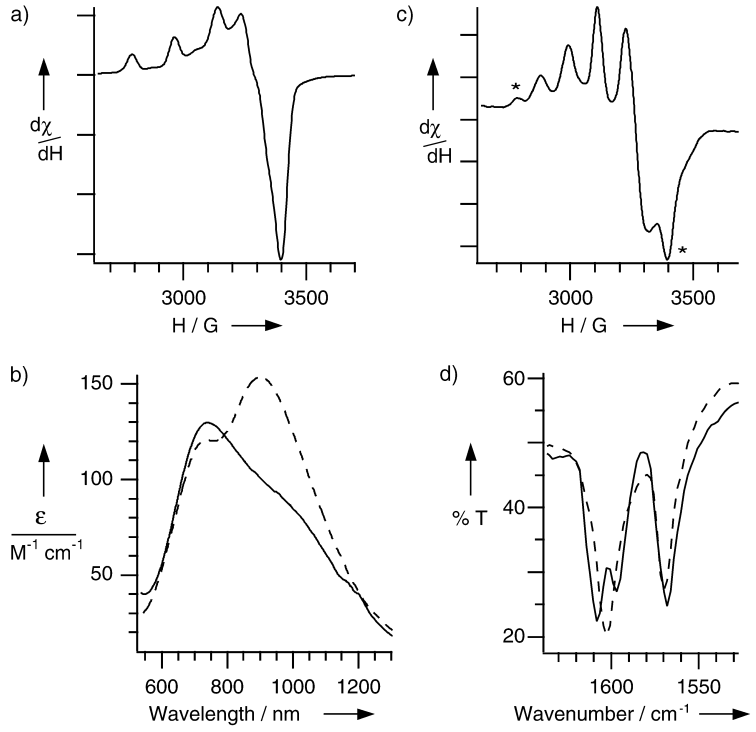

Figure 6. a–c) Controlled-potential electrolysis of $[Cu(H_2L^2)Cl_2]$ (**3**) in acetonitrile – 0.4 M $[NBu_4][PF_6]$ at +0.47 V (Pt gauze working electrode) to afford $[Cu(L^3)Cl]Cl$ (**4**): X-band EPR spectra of samples taken before (a) and after (c) the electrolysis and frozen at 80 K—the asterisks in c) mark peaks for residual **3** (see the text); b) UV-Vis-NIR spectra before (——) and after electrolysis (- - - -). d) Pyridyl-ring deformation bands from the FTIR spectra of $[Cu(H_2L^2)Cl_2]$ (**3**) (——) and isolated $[Cu(L^3)Cl]Cl$ (**4**) (- - - -).

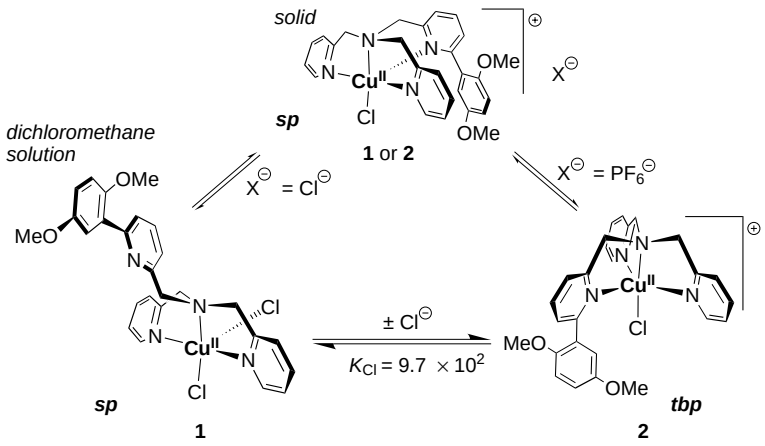

Scheme 1. $[Cu(L^1)Cl_2]$ (**1**) ⇄ $[Cu(L^1)Cl][PF_6]$ (**2**) equilibria.

tration[39] (Figure 5d) to be 9.7×10^2. The titration was also monitored by EPR spectroscopy with the spectrum of **1** replacing that of **2**, and a conductiometric titration of **2** with $[(Ph_3P)_2N]Cl$ gave an endpoint at 1.0 equivalents, corresponding to formation of the non-electrolyte **1**. For comparison, titrations in dichloromethane of $[Cu(tpa)Cl][PF_6]$ and of **4** with $[(Ph_3P)_2N]Cl$ (up to 20 equivalents) were investigated. In both cases no reaction was observed—as the increments of $[(Ph_3P)_2N]Cl$ were added, the EPR and Vis/NIR spectra of the solutions remained unchanged whereas the conductivity of the solutions monotonically increased. From these experiments the chloride binding constants of $[Cu(tpa)Cl][PF_6]$ and **4** in dichloromethane [Eq. (2)] are estimated to be both < 0.1.

Formation of 5 from 3: The EPR and the UV/Vis/NIR spectra described above for **3** were only obtained with some difficulty, by using carefully purified and rigorously dry solvents that have little Brønsted basicity such as dichloromethane, chloroform and acetonitrile, in which the complex was poorly soluble. The resulting blue-green solutions were extremely sensitive to trace amounts of moisture or other basic impurities, rapidly turning greenish-yellow to brown and with the characteristic EPR and UV/Vis/NIR spectra of **5** (see Supporting Information) replacing those of **3** if, for example, the solutions were exposed to moisture. Complex **3** was more soluble in alcohols such as methanol, but EPR and Vis/NIR spectra of these solutions show only peaks for **5**. These results highlight the non-innocence of the hydroquinonyl substituent in **3**—in the sense that it can coordinate to Cu—with solutions of **3** being difficult to obtain due to formation of **5** [Eq. (3): possible *base*s include a protonatable solvent or impurities]. The conductivity data for **3** and **5** in methanol, Table 2, are also consistent with this conclusion. Furthermore, a preliminary potentiometric titration of H_2L^2 and Cu^{2+} ion [as $Cu(ClO_4)_2$] in 95% methanol-water reveals one proton is lost from the ligand upon complex formation (to give **5**) which is complete above pH 2 with the value for the stability constant uncertain but high ($\log K > 15$).

$$[Cu(\kappa^3N\text{-}H_2L^2)Cl_2]\ (\mathbf{3}) + base \rightleftarrows [Cu(\kappa^3N\kappa O\text{-}HL^2)]^+\ (\mathbf{5}) + Hbase^+ + 2\ Cl^- \quad (3)$$

Electrochemistry: In the cyclic voltammograms (CVs) of complexes **1** and **2** in dichloromethane (see Supporting Information), the quasi-reversible (ΔE_p(couple) ~120–160 mV > $\Delta E_p(Fc^+ - Fc)$ ~65 mV with the scan rate = 100 mV s^{-1}), one-electron oxidations at +1.02 and +0.86 V, respectively, are attributed to the dimethoxyphenyl radical cation/dimethoxyphenyl couple.[40] The $Cu^{II} - Cu^{I}$ couples appear as a cathodic peak at −0.66 V for **1** and at −0.85 V for **2** with both complexes showing a broad anodic peak at about −0.5 V in the reverse sweep. The poor electrochemical

0947-6539/03/0901-0122 $ 20.00+.50/0 *Chem. Eur. J.* **2003**, *9*, No. 1

reversibility of the $Cu^{II}-Cu^{I}$ couples is indicative of the accompanying structural changes being rate-limiting on the CV time scale.[38, 41] A constant potential electrolysis of **1** at -0.95 V was a one-electron process and produced **6** (see above).

Cyclic voltammograms of H_2L^2 in acetonitrile are typical for a hydroquinonyl-containing compound and exhibit an anodic peak (**I**) at $+0.20$ V and a cathodic peak (**II**) at -0.59 V in the reverse sweep (Figure 7a). Peak **I** is attributed

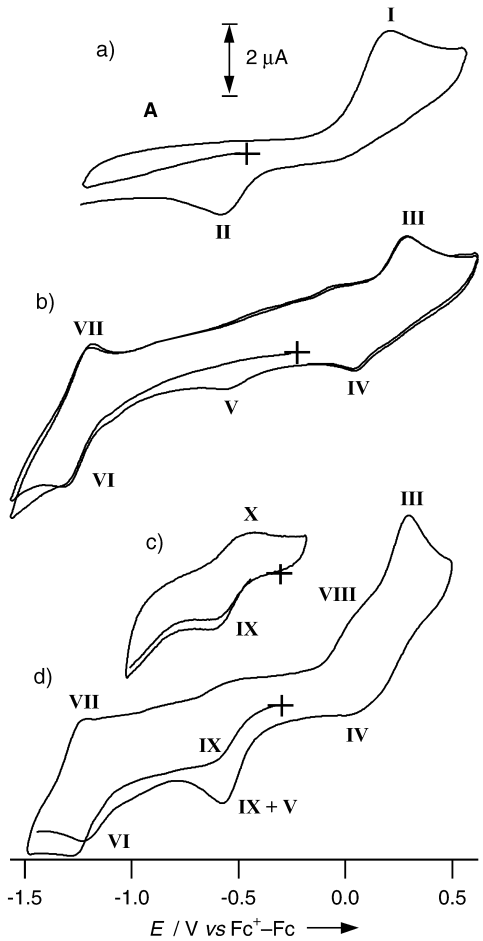

Figure 7. Cyclic voltammograms for: a) H_2L^2; b) $[Cu(HL^2)][PF_6]$ (**5**); c and d) $[Cu(H_2L^2)Cl_2]$ (**3**). Conditions: acetonitrile – 0.1 M $[Bu_4N][PF_6]$; 295 K; 1.0 mm Pt disk working electrode; scan rate = 100 mV s^{-1}.

to the anticipated hydroquinone-centred oxidation[29, 30] of H_2L^2 to afford quinone-substituted L^3 [Eq. (4)], and peak **II** to the reverse reduction process ($L^3/H^+ \rightarrow H_2L^2$). Although these processes are chemically reversible, they are electrochemically irreversible because the associated discharge or uptake of protons changes the local pH at the electrode.[29, 30]

$$H_2L^2 \rightleftarrows L^3 + 2H^+ + 2e^- \quad (4)$$

Figure 7b presents a representative CV for **5** in acetonitrile and reveals a quasi-reversible oxidation (the **III/IV** couple) at $+0.15$ V (ΔE_p(**III/IV**) ~ 260 mV cf. $\Delta E_p(Fc^+ - Fc) \sim 65$ mV at a scan rate (ν) = 100 mV s^{-1}; ΔE_p(**III/IV**) increases with ν) and a quasi-reversible reduction (the **VI/VII** couple) at -1.25 V [ΔE_p(**VI/VII**) ~ 105 mV at $\nu = 100$ mV s^{-1} and increases with ν). A comparison of the peak heights in the CVs of **2** (1 mM) and **5** (1 mM), both in acetonitrile, indicates both couples for **5** to be one-electron processes. Hence the reduction is attributed to a $Cu^{II}-Cu^{I}$ couple and the oxidation to a ligand-centred hydroquinonate – semiquinonate couple.[29, 30, 42] The quasi-reversibility of the couples may arise from concomitant rate-limiting structural changes. Also noteworthy in the CV of **5** is the cathodic "daughter" peak (**V**) at -0.57 V, which is found only after scanning through the **III/IV** couple. The potentials of peak **V** and peak **II**, which corresponds to reduction of L^3/H^+ in the CVs of H_2L^2, are very close and, accordingly, peak **V** is attributed to the reduction of a Cu^{II} species with a pendant quinone group. Such a species is expected: protonated semiquinones rapidly disproportionate,[19, 20, 29, 30] and disproportionation of the semiquinonate – Cu^{II} product of peak **III** would generate equal amounts of hydroquinonyl – Cu^{II} (**3** or **5**) and quinonyl – Cu^{II} species. The hydroquinonyl – Cu^{II} complexes (**3** or **5**) would be spontaneously oxidised at the potential of their formation (i.e., at all potentials higher than peak **III**),[19, 20, 29, 30] and therefore on the longer time scale of a bulk electrolysis **5** should undergo an overall two-electron oxidation to a quinonyl – Cu^{II} species. Consistent with this interpretation, controlled potential oxidation of **5** at $+0.40$ V consumed 1.94 Faraday mol^{-1}. Cyclic voltammograms of **5** in dichloromethane show qualitatively the same redox chemistry, but with redox couples at $+0.22$ and -1.08 V.

Cyclic voltammograms of **3** in acetonitrile (Figure 7c/d) reveal peaks **III/IV** and **VI/VII** for **5** as well as a quasi-reversible reduction couple (peaks **IX/X**) at -0.49 V (ΔE_p(**IX/X**) ~ 170 mV at $\nu = 100$ mV s^{-1} and increases with ν), which becomes less chemically reversible when the **VI/VII** couple is traversed, and an irreversible oxidation (peak **VIII**) at about 0.10 V. Vis/NIR and EPR spectra of the acetonitrile solutions were recorded prior to and after the CV experiments and show only peaks for **3** (Figure 6). The peaks for **5** in the CVs of **3** therefore suggest that pre-equilibration of **3** and **5** [Eq. (3)] occurs within the time scale of the CV experiment. Peaks **IX/X** are attributed to the $Cu^{II}-Cu^{I}$ couple for **3** with the accompanying structural changes being rate-limiting and leading to the quasi-reversible electrochemical response. Peak **VIII** is attributed to the two-electron oxidation anticipated for the "dangling" hydroquinone substituent in **3**, which should give the corresponding quinone in a chemically reversible, but electrochemically irreversible (proton-dependent) process;[20, 29, 30] thus oxidations of **3** (peak **VII**) and **5** (peak **III**) should both give quinonyl – Cu^{II} product. Supporting these conclusions, controlled potential electrolysis of **3** at $+0.47$ V consumed 1.97 Faraday mol^{-1}. Figure 6 depicts EPR and Vis/NIR spectra recorded prior to and after electrolysis of **3**—the spectra reveal **4** to be the electrolysis product (Scheme 2). The small peaks for a *sp* species—the axial subspectrum marked by asterisks—in the post-electrolysis EPR spectrum (Figure 6c) are attributed to residual **3** for two reasons: 1) They occur at identical magnetic field to peaks in the spectrum of **3**; 2) additional Cl^- ion did not affect the post-electrolysis UV/Vis/NIR or EPR spectra (Figure 6b/c), ruling out that they arise from the addition of Cl^- ion to **4** to give a

  0947-6539/03/0901-0123 $ 20.00+.50/0

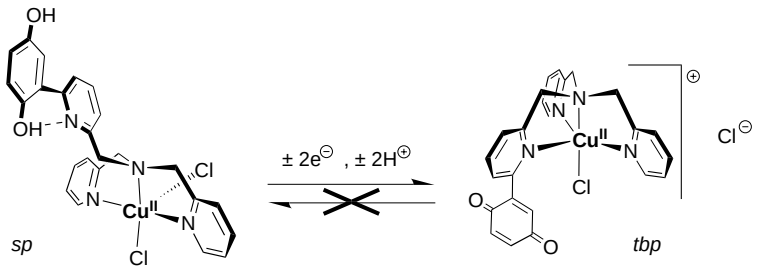

Scheme 2. Oxidation of *sp*-$[Cu(H_2L^2)Cl_2]$ (**3**) → *tbp*-$[Cu(L^3)Cl]Cl$ (**4**).

sp-quinonyl – Cu^{II} species. Cyclic voltammograms of **4**, produced by the electrolysis of **3**, revealed a broad cathodic peak at about -0.6 V in the forward cathodic sweep attributed to overlapping of the expected quinone- ($L^3/H^+ \rightarrow H_2L^2$)[20, 29, 30] and copper-($Cu^{II} \rightarrow Cu^{I}$) centred reduction processes, and in the reverse anodic sweep peak **X** and peak **VIII** as a "daughter" peak. The CV is typical for a basic quinone, which exhibit a cathodic peak for two-electron reduction of quinone/H^+ followed by a "daughter" anodic peak for two-electron oxidation of the corresponding hydroquinone in the reverse sweep rather than consecutive one-electron quinone/semiquinone anion and semiquinone anion/hydroquinone dianion couples, all due to extreme sensitivity to sub-equimolar amounts of Brønsted acids or hydrogen bond donors.[30] Controlled potential bulk electrolyses of **4** at -0.90 V caused decomposition and deposition of copper metal, a result suggestive for an unstable Cu^{I} product, such as **7** (see above), and consistent with the above assignment of the -0.6 V cathodic peak.

The $2e^-$, $2H^+$ quinone – hydroquinone couple may become electrochemically reversible in a buffered solution.[29, 30] Unfortunately, adding a pH-buffer to **3**, in aqueous or non-aqueous solvent, lead to complete conversion to **5** or, at very low pH (< 2), to decomplexation of H_2L^2; conditions could not be found where the **4-3** (hydro)quinone-centred couple was electrochemically reversible.

Copper(I) complexes

The Cu^{I} complexes **6** and **7** were not characterised by elemental analysis because of their extreme air-sensitivity. Positive ion ESI-mass spectra show strong peaks corresponding to the $[CuL]^+$ molecular ions, at *m/z* 490.0 (calcd: *m/z* 490.07) for **6** and *m/z* 462.0 (calcd: *m/z* 462.01) for **7**. The FTIR spectrum of solid **6** exhibits three prominent pyridine deformation bands indicative for an unbound, dangling PY* leg (Table 1).

The ^{1}H NMR spectra of **6** and **7** show several notable features. First, distinct coordination shifts ($\Delta\delta$) for the ligand protons are observed in the ^{1}H NMR spectra upon forming **6** and **7** (see Supporting Information). Second, the ^{1}H NMR spectra of the ligands and the complexes show two sharp methylene singlets, for example at $\delta_H(CD_3CN) = 4.07$ (2H) and 4.04 ppm (4H) for **6** and at $\delta_H(CD_3CN) = 4.00$ (2H) and 3.92 ppm (4H) for **7**, revealing the two 2-pyridylmethyl legs to be equivalent. However, the methylene protons of these legs are diastereotopic and should appear as a pair of AB methylene doublets as is found in ^{1}H NMR spectra of tpa complexes of substitutionally inert metal ions such as octahedral rhodium(III) complexes.[43] The methylene singlets in the ^{1}H NMR spectra of L^1, H_2L^2, **6** and **7** are accounted for by rapid inversion of configuration about the amine nitrogen, which is typically a low energy process for "free" amines.[44, 45] The methylene singlets remain sharp in NMR spectra of **6** recorded down to 260 K; based on this observation the estimated *upper limit* for the free energy barrier to exchange the diastereotopic methylene protons is about 45 kJ mol^{-1}. As a comparison, a variable temperature 300 MHz ^{1}H NMR study of the isoelectronic Zn^{II} complex, $[Zn(L^1)Cl_2]$, revealed a pair of AB doublets for the methylene protons in lower temperature spectra that coalesce ($T_{coalescence} = 290$ K) to a singlet in higher temperature spectra; the free energy barrier for intramolecular exchange of the diastereotopic methylene protons in this Zn^{II} complex is 56 ± 0.5 kJ mol^{-1}.[33]

Third, in the ^{1}H NMR spectra of H_2L^2 and **7** the hydroxy peaks appear as a sharp singlet at δ_H (CD_3CN) = 13.77 (H_2L^2) and 13.68 ppm (**7**) and a broad singlet at δ_H (CD_3CN) ~ 6.6 (H_2L^2) and ~ 9.9 ppm (**7**). The chemical shifts of the sharp low-field singlets show little concentration dependence indicative for an intramolecular hydrogen bond, which must be between the *ortho*-hydroxy group and the pyridyl nitrogen atom of the PY* leg. This strongly suggests that the PY* leg in **7** is unbound, akin to in the crystal structure of **3** (see above). Finally, the NMR peaks for **6** and **7** broaden slightly and shift when Cl^- ion was present or was deliberately added (data are presented in Table S1 in the Supporting Information), indicative for some association between the Cu^{I} centres and Cl^- ion.

In sum, these physicochemical data provide compelling evidence for a non-coordinated PY* leg in **6** and **7** in the solid state and in solution. Moreover, rapid inversion of the ligand configuration in **6** and **7** requires *at a minimum* dissociation of one of the three pyridylmethyl legs *and* the amine nitrogen atom (Scheme 3). The estimated upper limit of about 45 kJ mol^{-1} for exchange of the diastereotopic methylene protons in **6** compares with 28 ± 3 kJ^{-1} mol for the energy

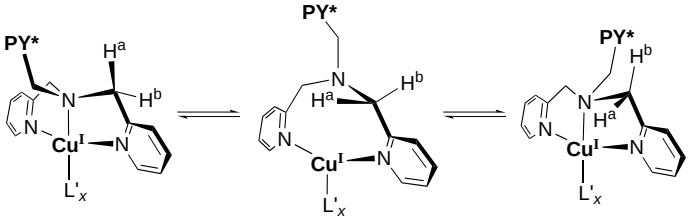

Scheme 3. Possible mechanism for exchange of the diastereotopic methylene protons in the Cu^{I} complexes, $[Cu(L)(L')_x]^{z+}$ (**6**: L = L^1, **7**: L = H_2L^2; L′ = ancillary (solvent or Cl^-) ligand), involving dissociation and inversion of the amine group.

0947-6539/03/0901-0124 $ 20.00+.50/0 *Chem. Eur. J.* **2003**, *9*, No. 1

barrier to inversion of configuration for dibenzylmethylamine,[45] which also provides an estimate for the lower limit to the barriers for inversion of configuration in "free" L^1 or "free" H_2L^2. Thus the barriers to amine inversion in **6** and **7** should fall in the range of about 30–45 kJ mol^{-1}, which compares with 56 kJ mol^{-1} for $[Zn(L^1)Cl_2]$[33] consistent with the ligand binding to Zn^{II} more strongly than to Cu^{I}.

Discussion

Towards the goal of preparing a copper–RHL system that provides "proof-of-concept" for our proposal for a redox-linked conformational proton pump gate operating as depicted in Figure 1, we have prepared a series of copper complexes of tpa ligands derivatised on one leg (PY*) by dimethoxyphenyl or (hydro)quinonyl groups. The redox states of the copper and (hydro)quinonyl centres and the environment control the geometries of the complexes (see Schemes 1 and 2). The interplay of the following effects is important:

1) *Steric interactions* introduced by the 6-aryl substitution of the PY* leg. These are minimised when the complexes adopt an *sp* geometry with the PY* leg in the weak-field, axial position (e.g. the *sp*-$[Cu(\kappa^4N\text{-}L^1)Cl]^+$ ion in the crystal structures of **1** and **2**) over a *tbp* geometry, and more so when the PY* leg is unbound (e.g. *sp*-$[Cu(\kappa^3N\text{-}H_2L^2)Cl_2]$ (**3**)) rather than bound. Intramolecular steric strain leads to hemilability—the fine balance between binding of the PY* leg versus Cl^- ion—in the **1**–**2** and **3**–**4** systems. In contrast, *tbp*-$[Cu(\kappa^4N\text{-tpa})Cl]^+$ is unaffected by excess Cl^- ion. In these complexes, the particular coordination geometry is unlikely to significantly influence whether or not a pyridyl leg undergoes substitution, because the ligand exchange reactions of five- (and lower[38]) coordinate Cu^{II} typically proceed by associative (*A*) or associative interchange (I_a) mechanisms and exhibit little dependence on the (*sp*–*tbp*) coordination geometry.[25]
2) *Electrostatic interactions*, which favour coordination of Cl^- over the PY* leg to copper; this effect is minimised in more polar/higher dielectric environments that better solvate ions and stabilise separation of charges. For **1**, a more polar medium, for example in the crystal or in a solvent with a higher dielectric constant such as dimethylformamide (ε_r (20 °C) = 38.3), stabilises separation of $[Cu(L^1)Cl]^+$ and Cl^- ions, whereas a less polar medium, for example in a solvent with a lower dielectric constant such as dichloromethane (ε_r (25 °C) = 8.9), promotes coordination of a second chloride coligand to afford $[Cu(\kappa^3N\text{-}L^1)Cl_2]$.
3) *Ligand field stabilisation energy* (LSFE) which increases upon binding of a π-acceptor pyridyl over a π-donor chloride coligand to the d^9 Cu^{II} ion. A comparison of **1** and $[Zn(L^1)Cl_2]$[33] reveals the importance of LFSE: whereas the crystal structure of **1** shows discrete $[Cu(\kappa^4N\text{-}L^1)Cl]^+$ and Cl^- ions, its Zn^{II} congener is $[Zn(\kappa^3N\text{-}L^1)Cl_2]$ because there is no LFSE for the d^{10} Zn^{II} ion and, in this case, minimisation of Coulombic and steric interactions leads to coordination of the second chloride coligand over the pendant PY* leg regardless of the medium.
4) *Perturbation of the donor properties of a ligand by an attached redox centre*: A comparison of *tbp*-$[CuCl(\kappa^4N\text{-}L^1)]^+$ (**2**) and *tbp*-$[CuCl(\kappa^4N\text{-}L^3)]^+$ (**4**), which differ only in the 6-substituent to PY*, reveals the importance of this effect. The d–d band maximum of **2** is about 370 cm^{-1} lower in energy than that for **4** because conjugation between the rings of the PY* legs results in L^3 being a stronger field ligand than L^1 (Figure 8A). The higher LFSE for **4** compared to **2** results in *tbp*-$[Cu(\kappa^4N\text{-}$

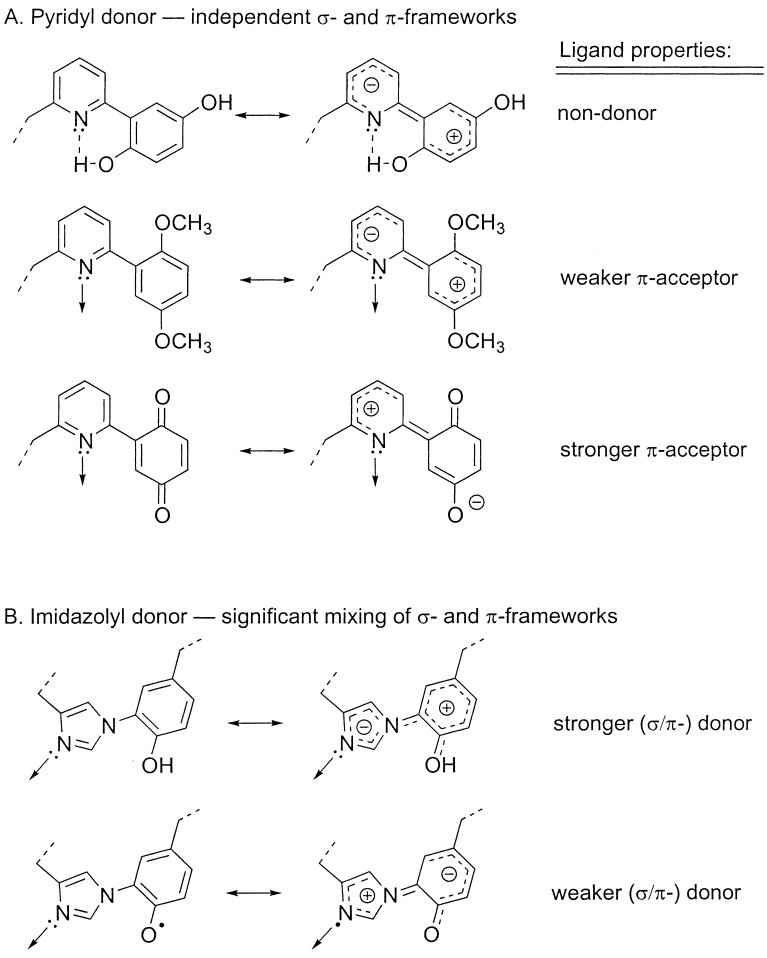

Figure 8. Redox-switched donor properties for hydroquinone/quinone-pyridine (A) and phenol/phenoxyl radical-imidazole (B) ligands.

  0947-6539/03/0901-0125 $ 20.00+.50/0

H_2L^3)Cl]$^+$ for **4** in the solid and in dichloromethane or acetonitrile, whereas **2** is *tbp*-[Cu(κ^4N-L^1)Cl]$^+$ in dichloromethane but *sp*-[Cu(κ^4N-L^1)Cl]$^+$ in the crystal. This in turn leads to the $>10^4$-fold difference in the affinities of the *tbp*-[Cu(κ^4N-L^1)Cl]$^+$ (from **2**) and *tbp*-[Cu(κ^4N-L^3)Cl]$^+$ (from **4**) ions for Cl^- ion in dichloromethane (see above), and hence to different structures when Cl^- ions are present—**2** binds Cl^- to give *sp*-[Cu(κ^4N-L^1)Cl_2] (**1**), whereas **4** does not.

5) *Intramolecular hydrogen bonding*, which may "tie-up" the σ-lone pair of a potential ligand group thereby stabilising "off"-Cu states (Figure 8A). That **3** is *sp*-[Cu(κ^3N-H_2L^2)Cl_2] in the crystal, whereas **1** crystallises as *sp*-[Cu(κ^4N-L^1)Cl]Cl, is attributed to the intramolecular hydrogen bond within the PY* leg of **3**.
6) *Oxidation state of copper*: Cu^I, along with other d^{10} metal ions, exhibits little preference for one type of donor or one particular geometry over another, and replacement of one donor of a tripodal ligand by an ancillary ligand is expected when this will reduce the repulsive and Coulombic forces.[41] Hence, the PY* leg is "dangling" in **6** and **7**—in acetonitrile this structure is likely stabilised by solvent binding to the Cu^I ion. A number of other Cu^I complexes of tpa-like ligands with bulky substituents, akin to in **6** and **7**, also exhibit an unbound ligand leg.[26]
7) *Availability of additional ligands*: Last, and implicit throughout the previous discussion, potential ancillary ligands must be available for the substitutionally labile PY* leg to be displaced from Cu^{II}; for example, the reaction of **2** with Cl^- ion to afford **1**. The shifts in the NMR spectra of **6** and **7** when Cl^- ion is introduced are indicative for association of Cl^- with the Cu^I centres.

A redox-driven switch in the conformation of a transition metal–RHL system tightly linked to proton uptake or output is critical to the successful operation of the proton pump gate proposed in Figure 1. The **3**–**4** system provides a first demonstration of this crucial step—the oxidation of **3** to **4** is linked to output of two protons and a switch of conformation from κ^3N- to κ^4N-bound ligand. Previous demonstrations of the use of a ligand-centred redox couple to switch the binding of the ligand to a transition metal centre are all for systems where the redox centre is directly bonded to the donor atom of the substitutionally labile group.[19–22] The **3**–**4** system clearly demonstrates for the first time that *the redox-state of a redox-centre covalently linked to a heterocyclic N-donor can control the binding of the N-donor to a metal ion.* The results also illustrate that redox-linked changes to hydrogen bonding may play an important role in the stabilisation of the different conformations for the labile, redox-active ligand group. Although complexes **3** and **4** could not be reversibly interconverted due to the formation of unstable Cu^I species and metal-binding by the hydroquinonyl redox group, the results provide a solid foundation for future studies toward artificial proton pumps.

As far as we are aware, a biological proton pump operating in the simple mode proposed in Figure 1 is yet to be discovered. Nevertheless, our results may have implications for biological systems. For instance, the structure-determining factors delineated in this study will also apply to biological copper centres with a substitutionally labile ligand. One such system is the Cu_B centre in cytochrome *c* oxidase,[4–13] which has a substitutionally labile histidine ligand proposed to be crucial to proton pumping by this enzyme.[6, 9] In this case, the substitutional lability would result from strain imposed by protein structure, perhaps with specific hydrogen bonding interactions between protein residues and the labile histidine stabilising the "off"-copper state, and with the displacement of the labile histidine requiring ancillary ligands (e.g. Cl^- or OH^- ion or water would need to be available to bind Cu_B) and more likely for the labile Cu_B(I) state. In the light of the present study, the facts that one histidine ligand to Cu_B is labile and that during the enzyme cycle the tyrosine–histidine ligand to Cu_B is oxidised with a hydroxide ancillary ligand simultaneously produced[6, 9, 12] become most intriguing. Argument based upon the mixing of σ/π electrons inherent within an imidazole[46] and the inter-ring conjugation anticipated for the tyrosine-histidine cofactor suggests its redox-state should strongly modulate its metal binding properties (Figure 8B). The most recent evidence is that there indeed is electronic delocalisation between the rings of a histidine–tyrosyl radical,[47] and we have shown that such inter-ring delocalisation between a ligand donor and its radical pendant can significantly alter the reactivity of a (organo-) metal centre.[48] The binding of the cofactor imidazole to Cu_B will be weakened by oxidation of the tyrosine, the converse to found for the pyridyl-based **3**–**4** system (Figure 8). Could it be that redox-triggered dissociation of the tyrosine-histidine cofactor from Cu_B is part of the mechanism of the proton pump in cytochrome *c* oxidase?[49] Further investigations are needed to address this important question.

Experimental Section

Physical measurements

Elemental analyses for C, H and N were determined by the Australian National University Microanalytical Unit. Electrospray ionisation mass spectra (ESI-MS) were acquired on a VG Quattro mass spectrometer with a capillary voltage of 4 kV and a cone voltage of 30 V. The solvent system was 50:50 acetonitrile/water and, depending on the sample, with or without 1% acetic acid. ^1H and $^{13}C\{^1H\}$ NMR spectra were recorded on a Bruker AC 300F (300 MHz) spectrometer. Electronic spectra of the complexes were recorded between 220 and 2000 nm on a CARY 5 spectrometer in the dual beam mode; solution spectra were recorded in sealed 1 cm quartz cuvettes and solid state spectra were recorded as KBr disks. Solutions of **3, 4, 6** and **7** were prepared under nitrogen in a M. Braun glovebox operating with dioxygen and water levels below 2 ppm. X-band EPR spectra of both frozen solution (at 80 K; liquid nitrogen dewar) and solid (dispersed in a KBr matrix) samples were recorded using a Bruker EMX 10 EPR spectrometer. Electrical molar conductivity measurements were made using an in-house built conductivity bridge and a YSI model 3403 conductivity cell thermostated at 25 °C. The cell constant (K) was determined with a standard aqueous solution of KCl (0.001 M). The molar conductivity, Λ_M, of a sample solution was determined from $\Lambda_m = 1000\ K/\ c_m$, where c_m is the molar concentration of the complex (ca. 1 mM).

Cyclic voltammetry measurements were made using a Pine Instrument Co. AFCBP1 bipotentiostat interfaced to and controlled by a Pentium computer as previously described in detail elsewhere.[20] Solutions of the compounds were 1.0 mM in anhydrous dichloromethane, acetonitrile or dimethylformamide (Aldrich, used as received) with 0.1M tetra-*n*-butylammonium hexafluorophosphate. Solutions were deoxygenated by bub-

0947-6539/03/0901-0126 $ 20.00+.50/0 *Chem. Eur. J.* **2003**, *9*, No. 1

bling with high purity nitrogen (presaturated with solvent) and then blanketed with a cover of nitrogen for the duration of the experiment or, alternatively, the electrochemical experiments were carried out in the above M. Braun nitrogen-filled glove-box. Data are reported from cyclic voltammograms recorded with a 1 mm Pt disk working electrode at a scan rate of 100 mV s^{-1}. Except where stated otherwise, electrochemical potentials herein are quoted relative to the ferrocenium–ferrocene ($Fe^{III}-Fe^{II}$) couple measured under the same experimental conditions (same concentrations, solvent, support electrolyte, electrodes, temperature, and scan rate).

Preparations

Preparation of bis(2-pyridylmethyl)[6-(2′,5′-dihydroxyphenyl)-2-pyridylmethyl]amine (H_2L^2): The preparation of H_2L^2 is described. The synthesis of L^1 employed a similar Suzuki coupling reaction, but is more straightforward and is described elsewhere.[33] Ligand H_2L^2 could not be obtained by reaction of L^1 with BBr_3.

1′,4′-Bis(tetrahydropyranyloxy)benzene: A suspension of 1,4-dihydroxybenzene (5.5 g, 50 mmol) in dichloromethane (125 mL) was treated with dihydropyran (12.6 g, 150 mmol) and pyridinium tosylate (250 mg, 1 mmol). After stirring for 3 h a clear solution was obtained, which was diluted with diethyl ether (250 mL) and washed with aqueous potassium hydroxide (20 mL, 5 %), until the aqueous layer was colourless. The organic layer was dried over anhydrous sodium sulfate and the solvent evaporated to give a white solid (13.8 g, ≈100 %), m.p. 98–99 °C; ^{1}H NMR (300 MHz, $CDCl_3$, 25 °C): $\delta = 6.97$ (s, 4H; Ph), 5.29 (m, 2H; THP), 3.93 (2H, m; THP), 3.58 (2H, m; THP), 1.99–1.96 (m, 2H; THP), 1.85–1.82 (m, 4H; THP), 1.64–1.58 ppm (m, 6H; THP); MS (70 eV): *m/z* (%): 278 (30) [M^+], 194 (10), 110 (100), 85 (65).

6-[2′,5′-Bis(tetrahydropyranyloxy)phenyl]-2-pyridylcarboxaldehyde: A solution of 1′,4′-bis(tetrahydropyranyloxy)benzene (2.0 g, 7.2 mmol) in THF (30 mL) was treated with *n*-butyllithium (3.5 mL (2.5 M in hexane), 8.5 mmol). After 2 h the solution was transferred using a cannula to a solution of triisopropylborate (3.5 mL, 15 mmol) in THF (5 mL) cooled to −80 °C. After 30 min, the temperature was allowed to rise to ambient and stirring was continued for 16 h. Evaporation of the solvent in vacuo gave a colourless oily residue. This was dissolved in toluene (40 mL), and 6-bromo-2-pyridylcarboxyaldehyde (1.4 g, 7.5 mmol), [$Pd(PPh_3)_4$] (0.4 g, 0.35 mmol), methanol (10 mL), and 2 M aqueous sodium carbonate (6 mL) were added. The mixture was heated at reflux for 8 h under nitrogen. After cooling, dichloromethane (50 mL), 2 M aqueous sodium carbonate solution (15 mL), and concentrated aqueous ammonia (2 mL) were added. The mixture was extracted with further dichloromethane, and the organic layer separated, dried over magnesium sulfate and the solvent removed using a rotary evaporator. Flash chromatography (silica support; dichloromethane/petroleum ether 3:1 eluent) of the residue yielded the product aldehyde as a pale yellow solid (1.6 g, 60 %), m.p. 76–77 °C; ^{1}H NMR (300 MHz, $CDCl_3$, 25 °C): $\delta = 10.15$ (s, 1H; CHO), 8.12 (m, 1H; Py), 7.88 (m, 2H; Py), 7.59 (s, 1H; Ph), 7.23 (s, 1H; Ph), 7.11 (s, 1H; Ph), 5.44 (m, 1H; THP), 5.36 (m, 1H; THP), 3.95 (m, 1H; THP), 3.82 (m, 1H; THP), 3.59 (m, 2H; THP), 2.05 (m, 2H; THP), 1.77 (m, 4H; THP), 1.61 ppm (6H, m; THP); IR (KBr disc): $\tilde{\nu} = 1735$ (C=O) cm^{-1}; MS (70 eV): *m/z* (%): 386 (2) [$M^+ + 1$], 299 (2.5), 215 (100).

Bis(2-pyridylmethyl){6-[2′,5′-bis(tetrahydropyranyloxy)phenyl]-2-pyridylmethyl}amine: 6-[2′,5′-Bis(tetrahydropyranyloxy)phenyl]-2-pyridylcarboxaldehyde (1.35 g, 5.1 mmol) and bis(2-pyridylmethyl)amine (1.0 g, 5 mmol) were dissolved in 1,2-dichloroethane (30 mL). Sodium triacetoxyborohydride (1.6 g, 7.55 mmol) was added. The solution was stirred overnight under nitrogen. The reaction was quenched with saturated aqueous sodium bicarbonate solution. The organic layer was separated, dried over anhydrous sodium sulfate, and the solvent was removed using a rotary evaporator to give a clear brown oil (2.35 g, 100 %); ^{1}H NMR (300 MHz, $CDCl_3$, 25 °C): $\delta = 8.55$ (d, 2H; Py), 7.72 (m, 6H; Py), 7.64 (m, 1H; Py), 7.50 (m, 1H; Py), 7.25–7.13 (m, 4H; Ph & Py), 7.03 (m, 1H; Ph), 5.39 (m, 1H; THP), 5.30 (m, 1H; THP), 3.94 (m, 4H; CH_2), 3.92 (s, 2H; CH_2), 2.05 (m, 2H; THP), 1.77 (m, 4H; THP), 1.61 ppm (m, 6H; THP); ESI-MS: *m/z* (%): 566 (10) [M^+], 482 (20), 398 (100).

H_2L^2: Aqueous 10 % hydrochloric acid solution was added dropwise to bis(2-pyridylmethyl)[6-(2′,5′-di-tetrahydropyranyloxyphenyl)-2-pyridylmethyl]amine (2.35 g, 4.15 mmol) in ethanol (40 mL) until pH 3. The solution was stirred at 55–60 °C for 3 h. The solvent was removed to near dryness on a rotary evaporator. The residue was extracted with dichloromethane (100 mL) and the extracts washed with saturated sodium bicarbonate (40 mL), then water (40 mL), and dried over sodium sulfate. Rotary evaporation of the solvent yielded a tacky yellow solid, which was recrystallised from chloroform/hexane to give a yellow powder (1.2 g, 63 %), m.p. 198–199 °C; ^{1}H NMR (300 MHz, $CDCl_3$, 25 °C) $\delta = 8.52$ (d, 2H; Py), 7.64 (m, 6H; Py), 7.36 (m, 1H; Py), 7.20 (m, 4H; Py), 7.13 (m, 2H; Ph), 6.90 (m, 1H; Ph), 3.90 (m, 4H; CH_2), 3.88 ppm (s, 2H; CH_2); elemental analysis calcd (%) for $C_{24}H_{22}N_4O_2 \cdot H_2O$: C 69.23, H 5.76, N 13.46; found: C 69.74, H 5.45; N 13.26.

[H_3L^2][ClO_4]: [*CAUTION*: Although no problems were encountered with this preparation, perchlorate salts are potentially explosive materials and appropriate precautions should be taken when handling them.] 40 % Aqueous $HClO_4$ was added dropwise to a solution of H_2L^2 (700 mg, 1.75 mmol) in 5 % water in ethanol solution (20 mL) until pH = 3.0. The yellow solid that precipitated was collected by filtration. Recrystallisation from ethanol/water gave clear yellow crystals of the product (700 mg, 80 %), m.p. 202–203 °C; ^{1}H NMR (300 MHz, [D_6]DMSO, 25 °C): $\delta = 8.62$ (d, 2H; Py), 7.92 (m, 4H; Py), 7.61 (d, 2H; Py), 7.45 (m, 3H; Py), 7.28 (m, 1H; Ph), 6.76 (m, 2H; Ph), 4.27 (s, 4H; CH_2), 4.21 ppm (s, 2H; CH_2); elemental analysis calcd (%) for $C_{24}H_{22}N_4O_2 \cdot HClO_4 \cdot H_2O$: C 55.76, H 4.84, N 10.84; found: C 55.98, H 4.85, N 10.83.

[$Cu(L^1)Cl$]Cl (1): L^1 (102 mg, 0.24 mmol) and $CuCl_2 \cdot 2H_2O$ (35 mg, 0.2 mmol) were dissolved in methanol (3 mL) and the solution was stirred for 10 min. Diethyl ether (15 mL) was then added, and the light blue microcrystalline solid which formed was collected by filtration and then recrystallized from methanol/diethyl ether to afford the blue crystalline product (115 mg, 95 %), m.p. 194 °C (decomp); X-band EPR (CH_2Cl_2, 80 K): $g_\parallel = 2.236$, $g_\perp = 2.027$, $A_\parallel = 176$ G; IR (KBr disc): $\tilde{\nu} = 3435$s, 2942w, 1608s, 1573s, 1498s, 1481m, 1455s, 1432s, 1399m, 1286s, 1206m, 1175w, 1096w, 1041m, 1028s, 890w, 875w, 819m, 801m, 782m, 721w, 655w cm^{-1}; UV/Vis/NIR (methanol): λ_{max} (ε) = 259 (14600), 311 (5070), 701 (100), 902 (75); UV/Vis/NIR (dichloromethane): λ_{max} (ε) = 257 (17700), 320 (8000), 770 (200), 1050 (130); ESI-MS: *m/z* (%): 548 (40) {[$Cu(L^1)(AcO)$]$^+$}, 526 (100) {[$Cu(L^1)Cl$]$^+$}, 489 (10), 427 (2), 245 (10); elemental analysis calcd (%) for $C_{26}H_{26}Cl_2CuN_4O_2 \cdot H_2O$: C 53.94, H 4.87, N 9.68; found: C 54.19, H 4.64, N 9.91.

[$Cu(L^1)Cl$][PF_6] (2): A solution of K[PF_6] (9.5 mg, 0.052 mmol) in methanol (2 mL) was added to [$Cu(L^1)Cl$]Cl (28 mg, 0.05 mmol) in methanol (5 mL). A pale blue precipitate formed which was recrystallised from dichloromethane/methanol to yield the blue microcrystalline product (28.4 mg, 85 %), m.p. 238 °C (decomp); X-band EPR (powder, 80 K): $g_1 = 2.22$, $g_2 = 2.07$, $g_3 \approx 2.0$ (br); X-band EPR (CH_2Cl_2, 80 K): $g_\perp = 2.235$, $g_\parallel \approx 2.0$, $A_\perp = 112$ G, $A_\parallel \approx 86$ G; IR (KBr disc): $\tilde{\nu} = 3445$br, 2940br, 1609s, 1581m, 1503s, 1461s, 1445s, 1293m, 1286m, 1265m, 1216s, 1163w, 1044s, 1023m, 876s, 816s, 774m, 557s cm^{-1}; UV/Vis/NIR (dichloromethane): λ_{max} (ε) = 259 (13500), 311 (6000), 730 (106), 930 (125); ESI-MS: *m/z* (%): 526 (100) {[$Cu(L^1)Cl$]$^+$}, 508 (40), 489 (20); elemental analysis calcd (%) for $C_{26}H_{26}N_4ClCuF_6O_2P$: C 46.58, H 3.91, N 8.36; found: C 46.19, H 3.86, N 8.30.

[$Cu(H_2L^2)Cl_2$] (3): Standing the dark green solution produced by mixing H_2L^2 (40 mg, 0.1 mmol) and $CuCl_2 \cdot 2H_2O$ (17 mg, 0.1 mmol) in ethanol (5 mL) under an atmosphere of diethyl ether gave jade green crystals of the product (40 mg, 75 %), m.p. 201 °C (decomp); X-band EPR (powder, 80 K): $g_1 = 2.17$, $g_2 = 2.13$, $g_3 = 2.04$; X-band EPR (CH_3CN, 80 K): $g_\parallel = 2.236$, $g_\perp = 2.027$, $A_\parallel = 176$ G; IR (KBr disc): $\tilde{\nu} = 3435$s, 3214s, 1608s, 1596s, 1567s, 1492s, 1470s, 1433m 1316m, 1283s, 1211s, 1166w, 1104w, 1052w, 1027m, 993w, 972w, 951w, 874w, 814s, 783s, 770s, 728m, 707m cm^{-1}; UV/Vis/NIR (acetonitrile): λ_{max} (ε) = 253 (16400), 336 (3600), 740 (130), 855 (120); ESI-MS: *m/z* (%): 460 (100) {[$Cu(HL^2)$]$^+$}; elemental analysis calcd (%) for $C_{24}H_{22}N_4Cl_2CuO_2 \cdot 1.5H_2O$: C 51.48, H 4.50, N 10.11; found: C 51.59, H 4.67, N 9.96.

[$Cu(L^3)Cl$]Cl (4): Three methods were employed to prepare this complex. The EPR, FTIR and UV/Vis/NIR spectral data for the product from each method were identical.

Method 1. Reaction of [$Cu(H_2L^2)Cl_2$] with DDQ: A solution of DDQ (1.08 mL, 49.5 mM) in dichloromethane (2 mL) was slowly added to a stirred suspension of [$Cu(H_2L^2)Cl_2$] (30 mg, 0.056 mmol) in dichloromethane (5 mL) cooled to −10 °C by an external coolant bath. The [$Cu(H_2L^2)Cl_2$] dissolved and an off-white precipitate formed ($DDQH_2$),

which was removed by filtration through a small pad of filter-aid to give a clear blue solution. Addition of an equal volume of diethyl ether caused the blue product to precipitate, which was collected by filtration and dried in vacuo (22 mg, 73 %), m.p. 120–122 °C; X-band EPR (powder, 80 K): $g_\perp \approx 2.2$ (br), $g_\parallel = 2.00$; X-band EPR (CH_2Cl_2, 80 K): $g_\perp = 2.228$, $g_\parallel \approx 2.0$, $A_\perp = 112$ G, $A_\parallel \approx 86$ G; IR (KBr disc): $\tilde{\nu} = 2940$s, 1659s, 1613s, 1564s, 1530s, 1455m, 1264s, 1173m, 1078w, 1054w, 1029w, 887m, 857w, 827w, 772m cm^{-1}; UV/Vis/NIR (CH_3CN): λ_{max} (ε) = 248 (10750), 277 sh (10700), 730 sh (120), 900 (150); UV/Vis/NIR (CH_2Cl_2): λ_{max} (ε) = 246 (10500), 265 sh (9800), 730 sh (100), 900 (130); elemental analysis calcd (%) for $C_{24}H_{20}N_4Cl_2CuO_2 \cdot H_2O$: C 52.51, H 4.04, N 10.21; found: C 52.78, H 4.04, N 9.93.

Method 2. Reaction of [Cu(H$_2$L^2)Cl$_2$] with cerium(IV) ammonium nitrate: A solution of $(NH_4)_2Ce(NO_3)_6$ (2.75 mL, 40.8 mM) in acetonitrile was added dropwise to a suspension of $[Cu(H_2L^2)Cl_2]$ (30 mg, 0.056 mmol) in acetonitrile (5 mL) cooled to −10 °C. The $[Cu(H_2L^2)Cl_2]$ dissolved affording a clear solution of $[Cu(L^3)Cl]Cl$, which was used for physical measurements. The spectroscopic data were identical to those for samples of $[Cu(L^3)Cl]Cl$ obtained by method 1 (or 3).

Method 3. Controlled potential oxidation of [Cu(H$_2$L^2)Cl$_2$]: This was carried out in a conventional three-compartment "H"-cell adapted so that it could be loaded and sealed under an inert atmosphere (high purity nitrogen). An acetonitrile-filled Ag/AgCl quasi-reference electrode (the same as used in CV experiments) was placed in the working compartment along with the Pt gauze (5×2 cm^2) working electrode and a Pt disk mini-electrode for running CV experiments. The counter electrode was a Pt gauze (4×2 cm^2) and was separated from the working compartment by two fine-porosity glass frits. During the electrolysis the solutions in the working compartment was stirred magnetically with a Teflon-coated stirring bar. Anhydrous acetonitrile (Aldrich) was used as the solvent, and the concentration of $[Cu(H_2L^2)Cl_2]$ was 2.0 mM and the support electrolyte was 0.2 M $[NBu_4][PF_6]$. The potential used was +0.47 V and was applied using the Pine potentiostat. The electrolysis consumed 1.97 Faraday mol^{-1}. Post-electrolysis electronic and EPR spectra are reproduced in Figure 6 and reveal that $[Cu(L^3)Cl]^+$ is produced.

[Cu(HL^2)][PF$_6$] (5): $[Cu(H_2L^2)Cl_2]$ (50 mg, 0.093 mmol) was dissolved in methanol (10 mL) containing NaOH (3.8 mg, 0.095 mmol). A brown solution formed and $K[PF_6]$ (18 mg, 0.1 mmol) in methanol was added to the aforementioned solution. After 15 min the solvent was removed yielding a brown solid that was recrystallised from acetone/diethyl ether to afford golden brown crystals of the product (42 mg, 75 %), m.p. 222 °C (decomp); X-band EPR (powder, 80 K): $g_\perp \approx 2.14$ (br), $g_\parallel = 2.01$; X-band EPR (CH_2Cl_2, 80 K) $g_\perp = 2.20$, $g_\parallel \approx 2.0$, $A_\perp = 115$ G, $A_\parallel \approx 84$ G; IR (KBr disc): $\tilde{\nu} = 3428$m, 3098m, 1608s, 1567m, 1463s, 1443s, 1408s, 1278s, 1219s, 1211s, 1180m, 1140w, 1105w, 1052w, 1020m, 841vs, 814m, 800m, 765s, 559s cm^{-1}; UV/Vis/NIR (CH_2Cl_2): λ_{max} (ε) = 232 (14600), 256 (13400), 286 (12000), 410 (4600), 523 (550), 650 (270), 1000 (90); ESI-MS: *m/z* (%): 460 (100) $\{[Cu(HL^2)]^+\}$; elemental analysis calcd (%) for $C_{24}H_{21}N_4CuO_2F_6P$: C 47.57, H 3.49, N 9.25; found: C 48.91, H 3.54, N 9.34.

[Cu(L^1)][PF$_6$] (6): In a nitrogen-filled glovebox, L^1 (42 mg, 0.1 mmol) was added to $[Cu(MeCN)_4][PF_6]$ (37 mg, 0.1 mmol) in CH_3CN (10 mL). A clear yellow solution formed. Removal of the solvent in vacuo afforded a pale-yellow solid (60 mg, 95 %); ^{1}H NMR (300 MHz, CD_3CN, 25 °C): $\delta = 8.44$ (d, 2H; Py), 7.72 (m, 3H; Py), 7.57 (m, 1H; Py), 7.30 (m, 5H; Py), 7.13 (m, 1H; Ph), 6.99 (m, 2H; Ph), 4.04 (s, 2H; CH_2), 3.98 (s, 4H; CH_2), 3.74 (s, 3H; OCH_3), 3.66 ppm (s, 3H; OCH_3); IR (KBr disc): $\tilde{\nu}$/cm^{-1} = 3063s, 1608s, 1597s, 1577s, 1523w, 1493s, 1460m, 1351m, 1322m, 1268 m, 1213s, 1079vs, 1011w, 854w, 818s, 622s; ESI-MS: *m/z* (%): 489 (25) $\{[Cu(L^1)]^+\}$, 427 (100).

[Cu(H$_2$L^2)][PF$_6$] (7): In a nitrogen-filled glovebox, H_2L^2 (40 mg, 0.1 mmol) was added to $[Cu(MeCN)_4][PF_6]$ (37 mg, 0.1 mmol) in CH_3CN (10 mL) to afford a clear yellow solution containing the product. ^{1}H NMR (300 MHz, CD_3CN, 25 °C): $\delta = 13.68$ (s, 1H; OH), ~9.9 (br s, 1H; OH), 8.50 (d, 2H; Py), 7.75–7.82 (m, 4H; Py), 7.26 (m, 6H; Py & Ph), 6.82 (m, 2H; Ph), 4.07 (s, 2H; CH_2), 3.96 ppm (s, 4H; CH_2); ESI-MS: *m/z* (%): 460 (100) $\{[Cu(H_2L^2)]^+\}$. Attempts to concentrate the solutions containing **7** resulted in disproportionation evidenced by the precipitation of copper metal and the solutions turning green due to formation of unidentified Cu^{II} species.

Crystallography

Relevant crystal, data collection and refinement data are summarised in Table 4. CCDC-175018—CCDC-175020 contain the supplementary crystallographic data for this paper. These data can be obtained free of charge via www.ccdc.cam.ac.uk/conts/retrieving.html (or from the Cambridge Crystallographic Data Centre, 12 Union Road, Cambridge CB2 1EZ, UK; fax: (+44) 1223-336033; or e-mail: deposit@ccdc.cam.ac.uk).

Acknowledgement

We are grateful to Professor L. F. Lindoy, the University of Sydney, for the Cu^{II} stability constant measurement for H_2L^2. This research was funded from an UNSW Vice-Chancellor's Goldstar Award (to S.B.C.).

[1] V. Balzani, A. Credi, F. M. Raymo, J. F. Stoddart, *Angew. Chem.* **2000**, *112*, 3484; *Angew. Chem. Int. Ed.* **2000**, *39*, 3349.
[2] J. K. Lanyi, A. Pohorille, *Biotech. Trends* **2001**, *19*, 140.
[3] D. G. Nicholls, S. J. Ferguson, *Bioenergetics 2*, Academic Press, London, **1992**.
[4] G. T. Babcock, M. Wikström, *Nature* **1992**, *356*, 301; S. Ferguson-Miller, G. T. Babcock, *Chem. Rev.* **1996**, *96*, 2889.
[5] S. Yoshikawa, K. Shinzawaitoh, R. Nakashima, R. Yaono, E. Yamashita, N. Inoue, M. Yao, M. J. Fei, C. P. Libeu, T. Mizushima, H. Yamaguchi, T. Tomizaki, T. Tsukihara, *Science* **1998**, *280*, 1723.
[6] M. Wikström, *Biochim. Biophys. Acta* **2000**, *1458*, 188.
[7] A. Aagaard, G. Gilderson, D. A. Mills, S. Ferguson-Miller, P. Brzezinski, *Biochemistry* **2000**, *39*, 15847.
[8] C. Ostermeier, A. Harrenga, U. Ermler, H. Michel, *Proc. Nat. Acad. Sci. USA* **1997**, *94*, 10547.
[9] M. Wikström, *Biochemistry* **2000**, *39*, 3515.

Table 4. Numerical crystal and refinement data for the X-ray crystal structures.

Complex	$[Cu(L^1)Cl]Cl \cdot 3H_2O$	$[Cu(H_2L^2)Cl_2]$	$[Cu(HL^2)][PF_6]$
formula (sum)	$C_{26}H_{32}Cl_2CuN_4O_5$	$C_{24}H_{22}Cl_2CuN_4O_2$	$C_{24}H_{21}CuF_6N_4O_2P$
M_w	615.0	532.9	606.0
crystal system	triclinic	monoclinic	monoclinic
space group	$P\bar{1}$	$P2_1/c$	$P2_1/c$
a [Å]	9.931(7)	7.270(3)	16.738(9)
b [Å]	14.798(12	25.539(5)	10.256(3)
c [Å]	19.716(15	13.153(5)	13.818(8)
α [°]	88.42(5)	90	90
β [°]	86.34(5)	106.14(2)	96.41(3)
γ [°]	75.87(6)	90	90
V [Å^3]	2804(4)	2346(1)	2357(2)
Z	4	4	4
μ [cm^{-1}] ($Cu_{K\alpha}$)	10.13	11.90	26.66
reflections collected	5637	4459	4614
R_{merge} (no. of equiv reflections)	0.020 (7)	0.017 (341)	0.056 (155)
observed reflections [$I/\sigma(I) > 3$]	3227	2494	2627
no. of parameters	344	298	309
observed reflections/no. parameters	9.4	8.4	8.5
final *R*, R_w [$I/\sigma(I) > 3$]	0.058, 0.078	0.033, 0.044	0.061, 0.087
goodness-of-fit	1.83	1.27	1.80
max., min. peaks in final difference map (e Å^{-3})	1.09, −0.66	0.44, −0.56	0.80, −0.71

[10] H. Michel, *Biochemistry* **1999**, *38*, 15129; D. Zaslavsky, R. B. Gennis, *Biochim. Biophys. Acta* **2000**, *1458*, 164.
[11] M. Ralle, M. L. Verkhovskaya, J. E. Morgan, M. I. Verkhovsky, M. Wikström, N. J. Blackburn, *Biochemistry* **1999**, *38*, 7185; J. P. Osborne, N. J. Cosper, C. M. V. Stalhandske, R. A. Scott, J. O. Alben, R. B. Gennis, *Biochemistry* **1999**, *38*, 4526.
[12] D. A. Proshlyakov, M. A. Pressler, G. T. Babcock, *Proc. Nat. Acad. Sci. USA* **1998**, *95*, 8020; D. A. Proshlyakov, M. A. Pressler, C. DeMaso, J. F. Leykam, D. L. DeWitt, G. T. Babcock, *Science* **2000**, *290*, 1588.
[13] D. M. Medvedev, I. Daizadeh, A. A. Stuchebrukhov, *J. Am. Chem. Soc.* **2000**, *122*, 6571.
[14] J. Jortner, M. Bixon, *Electron Transfer: From Isolated Molecules to Biomolecules,* Wiley, New York, **1999**.
[15] B. Eisenberg, *Acc. Chem. Res.* **1998**, *31*, 117; D. T. Bong, T. D. Clark, J. R. Granja, M. R. Ghadiri, *Angew. Chem.* **2001**, *113*, 1016; *Angew. Chem. Int. Ed.* **2001**, *40*, 988; G. W. Gokel, A. Mukhopadhyay, *Chem. Soc. Rev.* **2001**, *30*, 274; V. Sidorov, F. W. Kotch, G. Abdrakhmanova, R. Mizani, J. C. Fettinger, J. T. Davis, *J. Am. Chem. Soc.* **2002**, *124*, 2267.
[16] M. N. Paddon-Row, *Acc. Chem. Res.* **1994**, *27*, 18.
[17] D. Gust, T. A. Moore, A. L. Moore, *Acc. Chem. Res.* **2001**, *34*, 40.
[18] G. Steinberg-Yfrach, P. A. Liddell, S. C. Hung, A. L. Moore, D. Gust, T. A. Moore, *Nature* **1997**, *385*, 239; G. Steinberg-Yfrach, J. L. Rigaud, E. N. Durantini, A. L. Moore, D. Gust, T. A. Moore, *Nature* **1998**, *392*, 479.
[19] S. B. Sembiring, S. B. Colbran, D. C. Craig, *Inorg. Chem.* **1995**, *34*, 761.
[20] S. B. Sembiring, S. B. Colbran, D. C. Craig, *J. Chem. Soc. Dalton Trans.* **1999**, 1543.
[21] A. M. Allgeier, C. S. Slone, C. A. Mirkin, L. M. Liable-Sands, G. P. A. Yap, A. L. Rheingold, *J. Am. Chem. Soc.* **1997**, *119*, 550; C. S. Slone, C. A. Mirkin, G. P. A. Yap, I. A. Guzei, A. L. Rheingold, *J. Am. Chem. Soc.* **1997**, *119*, 10743; E. T. Singewald, C. A. Mirkin, C. L. Stern, *Angew. Chem.* **1995**, *107*, 1725; *Angew. Chem. Int. Ed.* **1995**, *34*, 1624.
[22] T. B. Higgins, C. A. Mirkin, *Chem. Mat.* **1998**, *10*, 1589; A. M. Allgeier, C. A. Mirkin, *Angew. Chem.* **1998**, *110*, 936; *Angew. Chem. Int. Ed.* **1998**, *37*, 894; D. A. Weinberger, T. B. Higgins, C. A. Mirkin, L. M. Liable-Sands, A. L. Rheingold, *Angew. Chem.* **1999**, *111*, 2748; *Angew. Chem. Int. Ed.* **1999**, *38*, 2565; D. A. Weinberger, T. B. Higgins, C. A. Mirkin, C. L. Stern, L. M. Liable-Sands, A. L. Rheingold, *J. Am. Chem. Soc.* **2001**, *123*, 2503.
[23] K. S. Chen, J. Hirst, R. Camba, C. A. Bonagura, C. D. Stout, B. K. Burgess, F. A. Armstrong, *Nature* **2000**, *405*, 814.
[24] H. M. N. H. Irving, R. J. P. Williams, *J. Chem. Soc.* **1953**, 3192.
[25] A. Neubrand, F. Thaler, M. Körner, A. Zahl, C. D. Hubbard, R. van Eldik, *J. Chem. Soc. Dalton Trans.* **2002**, 957; A. Pasquarello, I. Petri, P. S. Salmon, O. Parisel, R. Car, E. Toth, D. H. Powell, H. E. Fischer, L. Heim, A. E. Merbach, *Science* **2001**, *291*, 856.
[26] H. Nagao, N. Komeda, M. Mukaida, M. Suzuki, K. Tanaka, *Inorg. Chem.* **1996**, *35*, 6809; M. Harata, K. Hasegawa, K. Jitsukawa, H. Masuda, H. Einaga, *Bull. Chem. Soc. Jap.* **1998**, *71*, 1031.
[27] K. D. Karlin, S. Kaderli, A. D. Zuberbuhler, *Acc. Chem. Res.* **1997**, *30*, 139; M. Schatz, M. Becker, F. Thaler, F. Hampel, S. Schindler, R. R. Jacobson, Z. Tyeklar, N. N. Murthy, P. Ghosh, Q. Chen, J. Zubieta, K. D. Karlin, *Inorg. Chem.* **2001**, *40*, 2312; H. Hayashi, S. Fujinami, S. Nagatomo, S. Ogo, M. Suzuki, A. Uehara, Y. Watanabe, T. Kitagawa, *J. Am. Chem. Soc.* **2000**, *122*, 2124; C. He, J. L. DuBois, B. Hedman, K. O. Hodgson, S. J. Lippard, *Angew. Chem.* **2001**, *113*, 1532; *Angew. Chem. Int. Ed.* **2001**, *40*, 1484; A. Wada, M. Harata, K. Hasegawa, K. Jitsukawa, H. Masuda, M. Mukai, T. Kitagawa, H. Einaga, *Angew. Chem.* **1998**, *110*, 874; *Angew. Chem. Int. Ed.* **1998**, *37*, 798.
[28] Y. Naruta, T. Sasaki, F. Tani, Y. Tachi, N. Kawato, N. Nakamura, *J. Inorg. Biochem.* **2001**, *83*, 239; K. D. Karlin, A. D. Zuberbuhler in *Bioinorganic Catalysis,* 2nd ed. (Eds.: J. Reedjik, E. Bouwman), M. Dekker, **1999**, Chapter 14; R. A. Ghiladi, K. R. Hatwell, K. D. Karlin, H. W. Huang, P. Moënne-Loccoz, C. Krebs, B. Hanh Huynh, L. A. Marzilli, R. J. Cotter, S. Kaderli, A. D. Zuberbühler, *J. Am. Chem. Soc.* **2001**, *123*, 4515.
[29] J. Q. Chambers, in *The Chemistry of the Quinonoid Compounds, Vol. II,* (Eds.: Z. Rappoport, Z. Patai), Wiley, New York, **1988**, pp. 719–757.
[30] N. Gupta, H. Linschitz, *J. Am. Chem. Soc.* **1997**, *119*, 6384.
[31] A. F. Abdelmagid, K. G. Carson, B. D. Harris, C. A. Maryanoff, R. D. Shah, *J. Org. Chem.* **1996**, *61*, 3849.
[32] The oxygen reactivity is perhaps due to (intra- or inter-molecular) hydroquinone to copper(II) electron transfer to produce a copper(I)–semiquinone species, see: A. J. Evans, S. E. Watkins, D. C. Craig, S. B. Colbran, *J. Chem. Soc. Dalton Trans.* **2002**, 983; J. Rall, M. Wanner, M. Albrecht, E. M. Hornung, W. Kaim, *Chem. Eur. J.* **1999**, *5*, 2802.
[33] Z. He, S. B. Colbran, D. C. Craig, *J. Chem. Soc. Dalton Trans.* **2002**, 4224.
[34] A. W. Addison, A. N. Rao, J. Reedjik, J. Rijn, G. C. Verschoor, *J. Chem. Soc. Dalton Trans.* **1984**, 1349.
[35] P. Bhattacharyya, J. Parr, A. M. Z. Slawin, *J. Chem. Soc. Dalton Trans.* **1998**, 3263.
[36] S. J. Lange, H. Miyake, L. Que, Jr., *J. Am. Chem. Soc.* **1999**, *121*, 6330.
[37] M. M. da Mota, J. Rodgers, S. M. Nelson, *J. Chem. Soc. (A)* **1969**, 2036.
[38] B. J. Hathaway, in *Comprehensive Coordination Chemistry, Vol. 5* (Ed.: G. Wilkinson), Pergamon, Oxford, **1987**, pp. 533–774.
[39] K. A. Conners, *Binding Constants: The Measurement of Molecular Complex Stability*, Wiley-Interscience, New York, **1987**.
[40] A. Zweig, W. G. Hodgson, W. H. Jura, *J. Am. Chem. Soc.* **1964**, *86*, 4124; V. Le Berre, L. Angely, G. Simonet, G. Mousset, M. Bellec, *J. Electroanal. Chem.* **1987**, *218*, 273.
[41] E. A. Ambundo, M. V. Deydier, A. J. Grall, N. Aguera-Vega, L. T. Dressel, T. H. Cooper, M. J. Heeg, L. A. Ochrymowycz, D. B. Rorabacher, *Inorg. Chem.* **1999**, *38*, 4233.
[42] C. G. Pierpont, *Coord. Chem. Rev.* **2001**, *216*, 99.
[43] B. de Bruin, M. J. Boerakker, J. A. W. Verhagen, R. de Gelder, J. M. M. Smits, A. W. Gal, *Chem. Eur. J.* **2000**, *6*, 298; P. S. Aburel, C. Romming, K. Undheim, *J. Chem. Soc. Perkin Trans. 1.* **2001**, 1024.
[44] H. Kessler, *Angew. Chem.* **1970**, *82*, 237; *Angew. Chem. Int. Ed.* **1970**, *9*, 219.
[45] M. J. S. Dewar, W. B. Jennings, *J. Am. Chem. Soc.* **1971**, *93*, 401.
[46] H. M. Marques, O. Q. Munro, T. Munro, M. de Wet, P. R. Vashi, *Inorg. Chem.* **1999**, *38*, 2312; A. R. Katritzky, K. Jug, D. C. Oniciu, *Chem. Rev.* **2001**, *101*, 1421.
[47] J. A. Cappuccio, I. Ayala, G. I. Elliott, I. Szundi, J. Lewis, J. P. Konopelski, B. A. Barry, O. Einarsdóttir, *J. Am. Chem. Soc.* **2002**, *124*, 1750.
[48] W. M. Harrison, C. Saadeh, S. B. Colbran, *Organometallics* **1997**, *16*, 4254.
[49] In this scenario a role for the covalent link within the His 240-Tyr 244 cofactor would be to ensure the redox-triggered dissociation of His 240 from Cu_B upon oxygen binding drives helix distortion, which would provide an attractive mechanism for storing the energy for proton pumping in the later steps (during the reductive phase) of the enzyme's catalytic cycle: S. B. Colbran, M. N. Paddon-Row, unpublished results.

Received: May 8, 2002 [F4077]